AD-A193 017 GUIDED WAVE INTERACTIONS IN MILLIMETER-WAVE INTEGRATED CIRCUITS(U) TEXAS UNIV AT AUSTIN DEPT OF ELECTRICAL AND COMPUTER ENGINEERING T ITOH 15 JAN 88 ARO-21430.41-EL 1/1

UNCLASSIFIED DAAG29-84-K-0076 F/G 9/1 NL

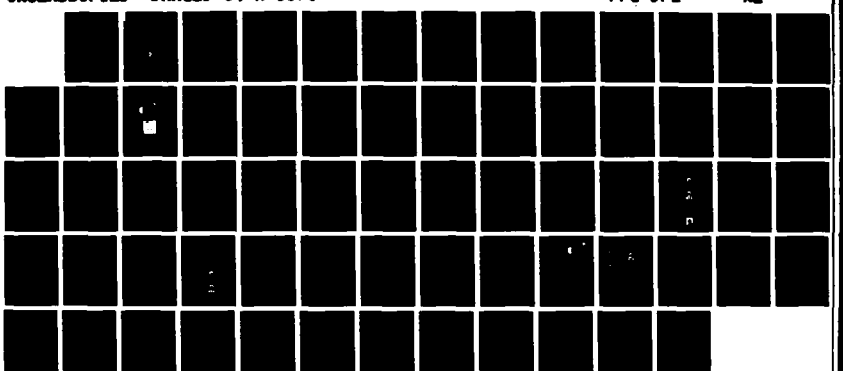

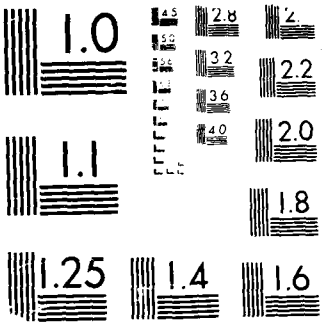

ARO 21438.41-EL

(2)

# Guided Wave Interactions in Millimeter-Wave Integrated Circuits



Final Report

by

Tatsuo Itoh

January 15, 1988

U.S. Army Research Office

Contract No.: DAAG29-84-K-0076

The University of Texas at Austin
Department of Electrical and Computer Engineering
Austin, Texas 78712



APPROVED FOR PUBLIC RELEASE:
DISTRIBUTION UNLIMITED

UNCLASSIFIED
SECURITY CLASSIFICATION OF THIS PAGE

# REPORT DOCUMENTATION PAGE

| | |
|---|---|
| 1a. REPORT SECURITY CLASSIFICATION<br>Unclassified | 1b. RESTRICTIVE MARKINGS |
| 2a. SECURITY CLASSIFICATION AUTHORITY | 3. DISTRIBUTION / AVAILABILITY OF REPORT<br>Approved for public release; distribution unlimited. |
| 2b. DECLASSIFICATION / DOWNGRADING SCHEDULE | |
| 4. PERFORMING ORGANIZATION REPORT NUMBER(S) | 5. MONITORING ORGANIZATION REPORT NUMBER(S) |
| 6a. NAME OF PERFORMING ORGANIZATION<br>The University of Texas at Austin<br>6b. OFFICE SYMBOL (*If applicable*) | 7a. NAME OF MONITORING ORGANIZATION<br>U. S. Army Research Office |
| 6c. ADDRESS (*City, State, and ZIP Code*)<br>Department of Electrical & Computer Engineering<br>The University of Texas<br>Austin, TX 78712 | 7b. ADDRESS (*City, State, and ZIP Code*)<br>P. O. Box 12211<br>Research Triangle Park, NC 27709-2211 |
| 8a. NAME OF FUNDING / SPONSORING ORGANIZATION<br>U. S. Army Research Office<br>8b. OFFICE SYMBOL (*If applicable*) | 9. PROCUREMENT INSTRUMENT IDENTIFICATION NUMBER |
| 8c. ADDRESS (*City, State, and ZIP Code*)<br>P. O. Box 12211<br>Research Triangle Park, NC 27709-2211 | 10. SOURCE OF FUNDING NUMBERS<br>PROGRAM ELEMENT NO. / PROJECT NO. / TASK NO. / WORK UNIT ACCESSION NO |
| 11. TITLE (*Include Security Classification*)<br>Guided Wave Interactions in Millimeter-Wave Integrated Circuits | |
| 12 PERSONAL AUTHOR(S)<br>Tatsuo Itoh | |
| 13a. TYPE OF REPORT<br>Final Report<br>13b. TIME COVERED<br>FROM 9/1/84 TO 1/15/88 | 14. DATE OF REPORT (*Year, Month, Day*)<br>Jan. 15, 1988<br>15. PAGE COUNT<br>56 |
| 16 SUPPLEMENTARY NOTATION<br>The view, opinions and/or findings contained in this report are those of the author(s) and should not be construed as an official Department of the Army position, policy, or decision, unless so designated by other documentation. | |
| 17 COSATI CODES<br>FIELD / GROUP / SUB-GROUP | 18. SUBJECT TERMS (*Continue on reverse if necessary and identify by block number*)<br>planar transmission line structures, quasi-optical components, slow-wave structures, optical interactions, active device modeling |

19 ABSTRACT (*Continue on reverse if necessary and identify by block number*)

This report summarizes activities in the Electrical Engineering Research Laboratory at The University of Texas on various structures for millimeter-wave circuits. This work was done under the sponsorship of the U.S. Army Research Office under Contract DAAG29-84-K-0076. The topics of investigation included planar transmission line structures, quasi-optical components, slow-wave structures, optical interactions and active device modeling. A list of publications is included.

| | |
|---|---|
| 20 DISTRIBUTION / AVAILABILITY OF ABSTRACT<br>☐ UNCLASSIFIED/UNLIMITED ☐ SAME AS RPT. ☐ DTIC USERS | 21. ABSTRACT SECURITY CLASSIFICATION<br>Unclassified |
| 22a. NAME OF RESPONSIBLE INDIVIDUAL | 22b. TELEPHONE (*Include Area Code*) / 22c. OFFICE SYMBOL |

DD FORM 1473, 84 MAR — 83 APR edition may be used until exhausted. All other editions are obsolete.

SECURITY CLASSIFICATION OF THIS PAGE
UNCLASSIFIED

# Guided Wave Interactions in Millimeter-Wave Integrated Circuits

Final Report

by

Tatsuo Itoh

January 15, 1988

U.S. Army Research Office

Contract No.: DAAG29-84-K-00766

The University of Texas at Austin
Department of Electrical and Computer Engineering
Austin, Texas 78712

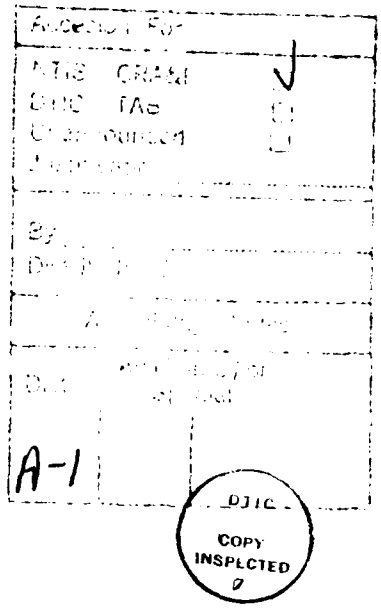


APPROVED FOR PUBLIC RELEASE:
DISTRIBUTION UNLIMITED

## TABLE OF CONTENTS

## APPENDICES

Appendix 1 "Comparative Study of Mode-Matching Formulations for Microstrip Discontinuity Problems," T. S. Chu, T. Itoh, Y.-C. Shih, IEEE Transactions on Microwave Theory and Techniques, Vol. MTT-33, No. 10, October 1985.

Appendix 2 "Generalized Scattering Matrix Method for Analysis of Cascaded and offset Microstrip Step Discontinuities," T.S. Chu and T. Itoh, IEEE Transactions on Microwave Theory and Techniques, Vol. MTT-34, No. 2, February 1986.

Appendix 3 "Microstrip-Fed Planar Frequency-Multiplying Space Combiner," S. Nam, T. Uwano, T. Itoh, IEEE Transactions on Microwave Theory and Techniques, Vol. MTT-35, No. 12, December 1987.

Appendix 4 "Crosstie Overlay Slow-Wave Structure for Broadband Traveling-Wave Type Electro-Optical Moculators," H.-Y. Lee, T.H. Wang, T. Itoh (submitted to International Journal of Infrared and Millimeter Waves).

## ABSTRACT

This report summarizes activities in the Electrical Engineering Research Laboratory at The University of Texas on various structures for millimeter-wave circuits. This work was done under the sponsorship of the U. S. Army Research Office under Contract DAAG29-84-K-0076. The topics of investigation included planar transmission line structures, quasi-optical components, slow-wave structures, optical interactions and active device modeling. A list of publications is included.

## 1. Introduction

As the operating frequency of the millimeter-wave circuits is increased, some of the problems that are not very relevant at lower frequencies become significant. For instance, accurate evaluations of the discontinuities in the planar transmission lines become essential in the design of the integrated circuits, particularly those in the monolithic form. It is no longer sufficient to simply characterize the active device from the DC point of view. Interactions of the guided waves with the active devices becomes important in the design of many components. It is desirable and necessary to explore new types of circuits and structures that take advantages of these wave interactions.

The projects summarized in this report have been undertaken with the spirit mentioned above. A number of projects on the interactions of the guided waves with devices have been studied. This report summarizes all of the projects supported by the Army Research Office under Contract DAAG29-84-K-0076 and the publications that resulted.

## 2. Planar Transmission Lines

In the past several years, numerous publications have appeared in the literature on the subject of guided wave characteristics of various planar transmission lines. In spite of all this activity, accurate characterizations of discontinuities as the frequency is increased are still in a rather primitive stage . Additionally, a recent discovery has generated some interest in superconducting planar transmission lines. Projects related to these subjects will be summarized below.

### 2.1 Microstrip Step Discontinuities

The microstrip step discontinuity problems are often formulated in terms of the mode matching technique applied to an equivalent waveguide model. Figure 1 shows the step discontinuity as analyzed by the mode matching technique. From the mode matching

technique, several different formulations are obtained depending on how the E- and H-field continuity equations are processed. Some formulations are believed to be superior to others in terms of convergence and numerical labor. An extensive study has been conducted to compare all possible formulations for the microstrip discontinuity problem. It was found that one of them is much superior to all others. In fact, this is the simplest formulation and requires the smallest matrix [1] (see Appendix 1). To study the accuracy of the method, an independent check of the results has been conducted by using the Modified Residue Calculus Technique. This method is known to be numerically efficient and to result in accurate scattering parameters of the discontinuity. The results compare very well with those obtained using the mode matching method as well as those that have been reported in the literature [2].

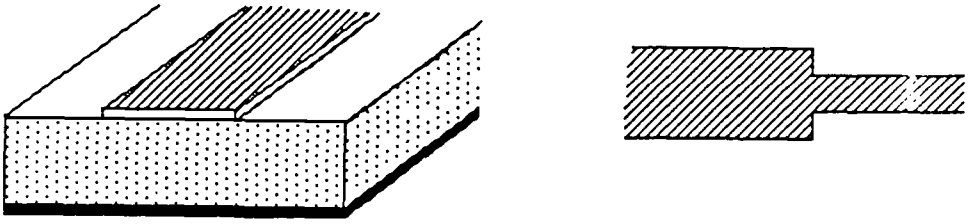

Fig.1. Microstrip Step Discontinuity

When the mode matching method or the Modified Residue Calculus Technique is combined with the Generalized Scattering Matrix Technique, cascaded and offset step discontinuities can be characterized. The cascaded step discontinuities often appear in the form of a symmetric stub to the main microstrip line and can be decomposed to two

successive step discontinuities. On the other hand, the offset microstrip discontinuity can be decomposed to two successive step discontinuities separated by a zero distance. First, each step discontinuity is characterized by the mode matching method or by the Modified Residue Calculus Technique so that the generalized scattering matrix of each discontinuity is derived. These generalized scattering matrices are combined by the matrix manipulation to obtain that of the composite structure. The interactions between the two discontinuities by way of the dominant as well as higher order modes are taken into account [3] (see Appendix 2).

## 2.2 Non-Touching E-Plane Fin and Its Application to an Evanescent Mode Filter

A non-touching E-plane fin shown in Fig.2 is a useful circuit component for E-plane integrated circuits. It is printed on a sustrate which is in turn inserted into a $TE_{10}$ waveguide along its E-plane. One end of the stub is connected to the top or bottom wall of the waveguide whereas another end does not reach the opposite wall. This element can be used as a transition from a waveguide to a printed circuit and as a filter element. This configuration has been analyzed by an extension of the spectral domain technique. This extension essentially provides a Fourier transformed version of the integral equations with respect to unknown current components excited on the stub. The formulations are algebraic equations with inhomogeneous terms corresponding to the incident mode. These equations are solved for the current components on the stub. Once these current components are found, the amplitude of a particular scattered mode can be identified from the residue of the Green's function in the spectral domain [4,5].

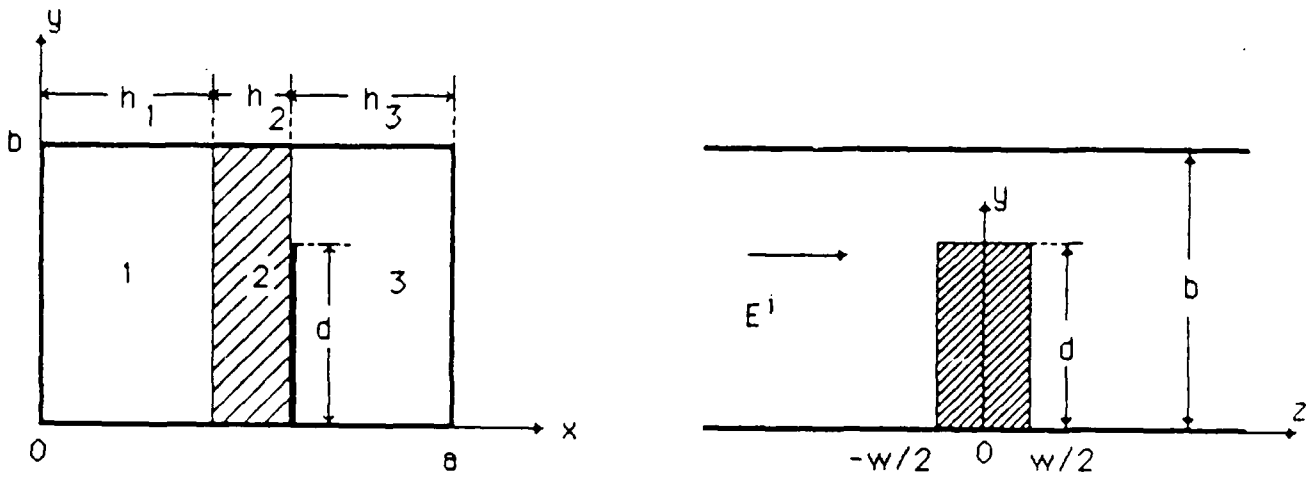


Fig.2. Non-Touching E-Plane Fin

The analysis is extended to the case where a non-touching E-plane fin is located in the waveguide below cutoff. With this configuration, an evanescent mode filter can be formed. The evanescent waveguide containing non-touching E-plane fins are connected to the standard waveguides on both ends via double step discontinuities as shown in Fig. 3. The generalized scattering parameters are obtained for the double step discontinuity by means of the mode matching method. Each fin is characterized by the extended spectral domain method and the generalized scattering parameters are obtained. Connecting all of these scattering matrices, one can find the scattering matrix of the entire filter. A simple way of explaining the operation of this filter is as follows. The waveguide below cutoff is essentially a quasi-lumped inductance. The non-touching E-plane fin provides a capacitance which resonates with the inductance to determine the passband of the filter [6]. A typical passband characteristic is shown in Fig. 4.

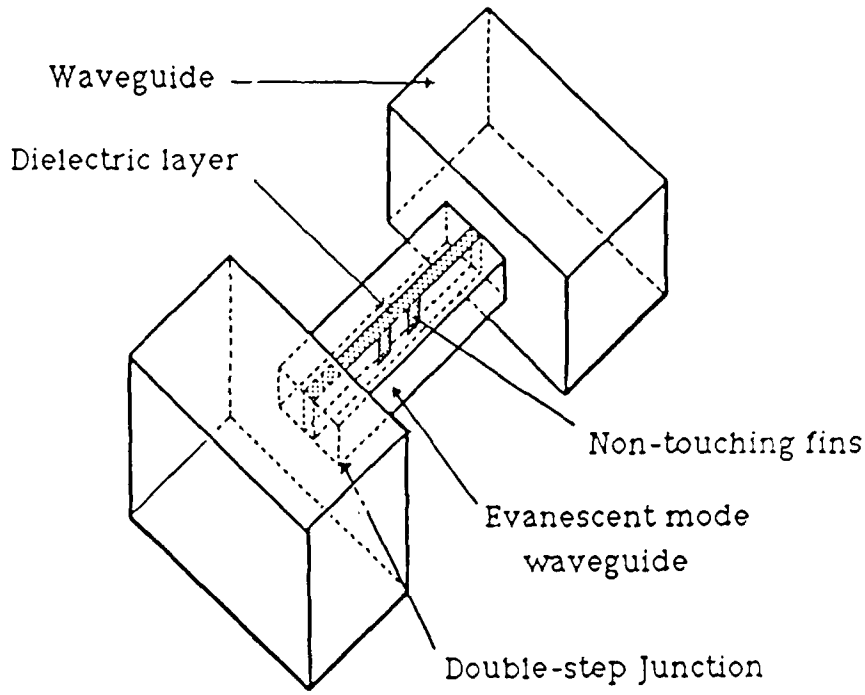


Fig.3. Evanescent Mode Filter

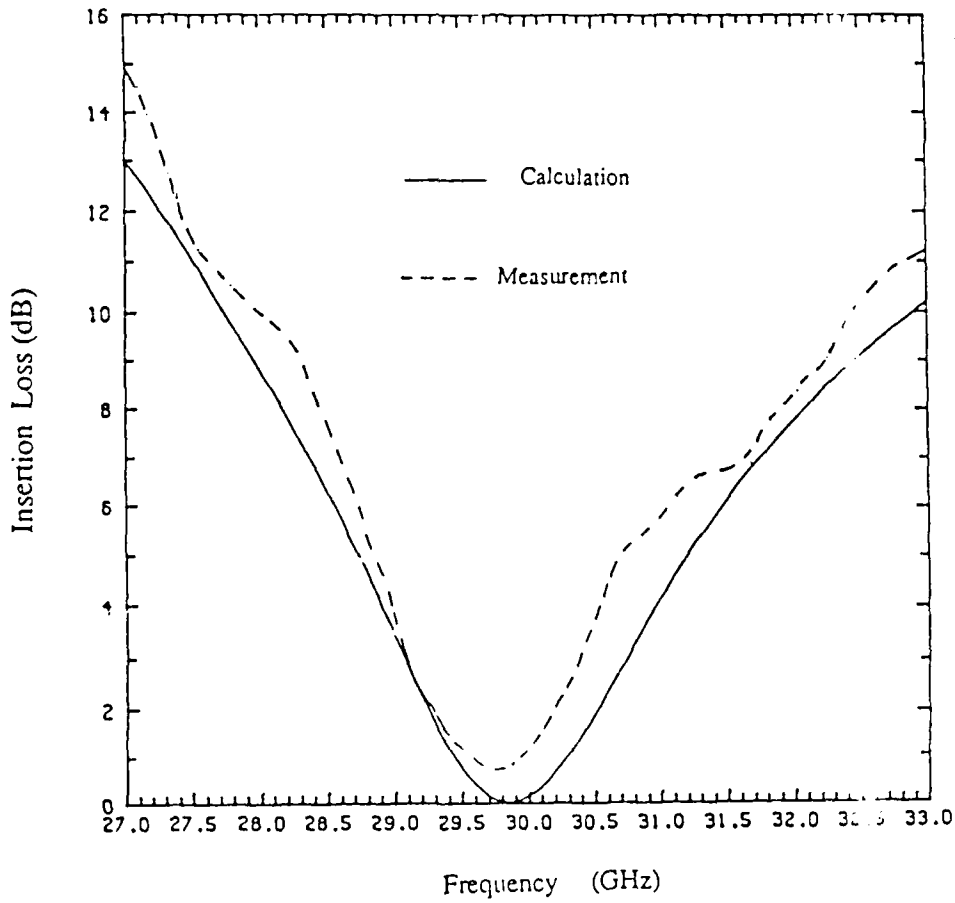


Fig. 4. Passband Characteristic of an Evanescent Mode Filter

2.3 Finline With a Ferrite Layer

A finline with a ferrite substrate can be used for a nonreciprocal phase shifter. However, this structure is not very practical. A more practical one uses a dielectric substrate and a ferrite layer is attached on the unmetalized side of the substrate as shown in Fig. 5. In this manner, design flexibility can also be increased. This structure has been analyzed by the spectral domain method. It is found that an appropriate choice of structural parameters can enhance nonreciprocity of the phase velocity. Hence, the nonreciprocal phase shifter based on the present structure can be optimized [7].

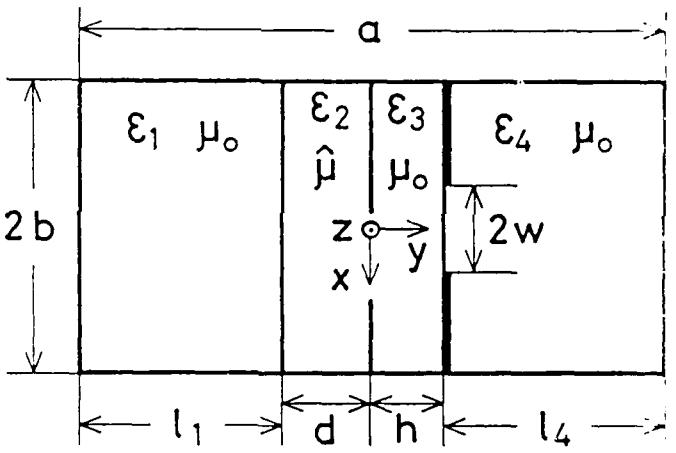


Fig. 5. Ferrite Loaded Finline

2.4. Superconducting Planar Transmission Lines

Although the resistance in a superconductor is zero at DC, it is not zero at higher frequencies due to penetration depth. Nevertheless, the conductor loss in a superconducting planar transmission line is substantially smaller than its counterpart in the normal metal transmission line. Therefore, the dielectric loss is the dominant loss mechanism for the wave attenuation. The extent of the dielectric loss has been

investigated and several modifications of the microstrip line have been suggested for possible dielectric loss reduction [8].

## 3. Quasi-Optical Structures

As the operating frequencies are increased, a quasi-optical structure is an attractive alternative for conventional microwave and millimeter-wave systems. A typical quasi-optical system consists of lenses, reflectors and wire grids. The wave in these free-space waveguides eventually interface with microwave circuits. In the past several years, there have been some efforts to use planar circuit technology in this interfacing portion of the structure. A number of quasi-optical mixers have been reported in which a planar antenna is directly integrated with the mixer circuit [9,10]. In comparison to these mixers, little has been reported on studies of other active components. Several attempts have been made in this area during this contract period.

### 3.1 Planar Frequency-Doubling Space Power Combiner

A novel structure for a high-power millimeter-wave quasi-optical application has been conceived and tested. On a large ground plane, a number of periodically placed slots are created and a varactor or Schotkky diode is placed in each solt. These slots are excited by a reduced height waveguide with its top wall as a part of the ground plane described above (see Fig. 6.). The slots are resonant at the desired second harmonic frequency and fed by the fundamental frequency from the reduced height waveguide. Since the slots are electrically small at the fundamental frequency, only a small amount is coupled to each slot. Thus, a large number of slots can be fed by a single source. No branching network or tuning circuits are required. The diode can be operated without any dc bias. The second harmonic signals from each slot are radiated into free space and combined there. In a test from 4 to 8 GHz multiplication, the conversion loss is about 2 dB and in the one from 17 to 34 GHz it is 7 dB. Fourteen diodes are used in the

structure and the sidelobe level of this "phased array" is less than -14 dB. An 8-diode combiner has been tested for doubling a 35 GHz signal to a 70 GHz output and the sidelobe level was less than -12 dB [11].

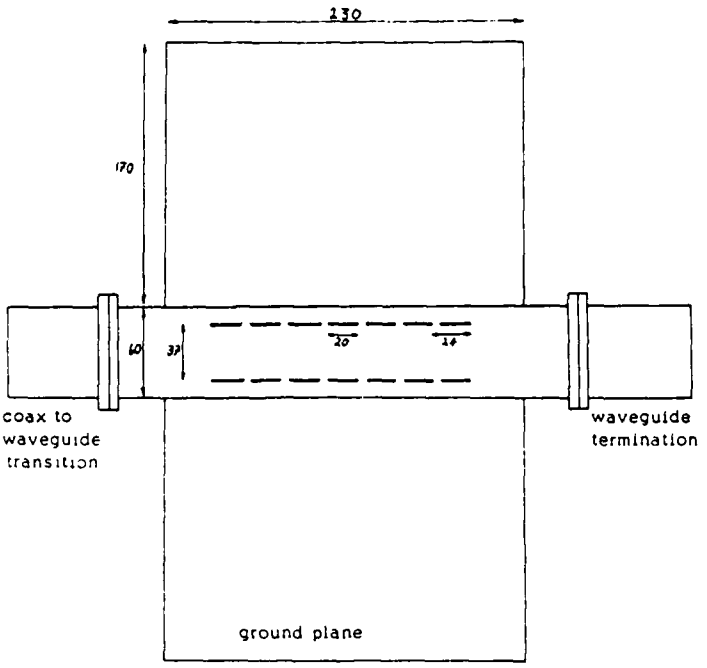


Fig.6. Quasi-Optical Multiplying Slot Combiner Array

3.2 Planar Frequency-Doubling Power Combiner Excited by a Microstrip Line

The frequency-doubling power combiner is fed by a microstrip in this project so that the structure is more amenable to planar and, eventually, to monolithic fabrication. In this structure, a number of slots in the ground plane on the substrate are excited by a microstrip line on the other side of the substrate (see Fig. 7). First, characteristics of the transition from a microstrip line to a quarter wave slot has been studied. From this study, the amount of power left over to the output side of the microstrip line can be evaluated. The location of the transition is adjusted at each slot so that approximately the same amount of power is fed to each slot. Also, the length of the microstrip line feed between the two slots is adjusted so that all the slots are fed in phase. Based on these studies, slot

arrays with up to eight elements have been successively tested. The conversion loss was about 16 dB from the input of 5.4 GHz to the output of 10.8 GHz [12]. A detailed design consideration is reported in Appendix 3.

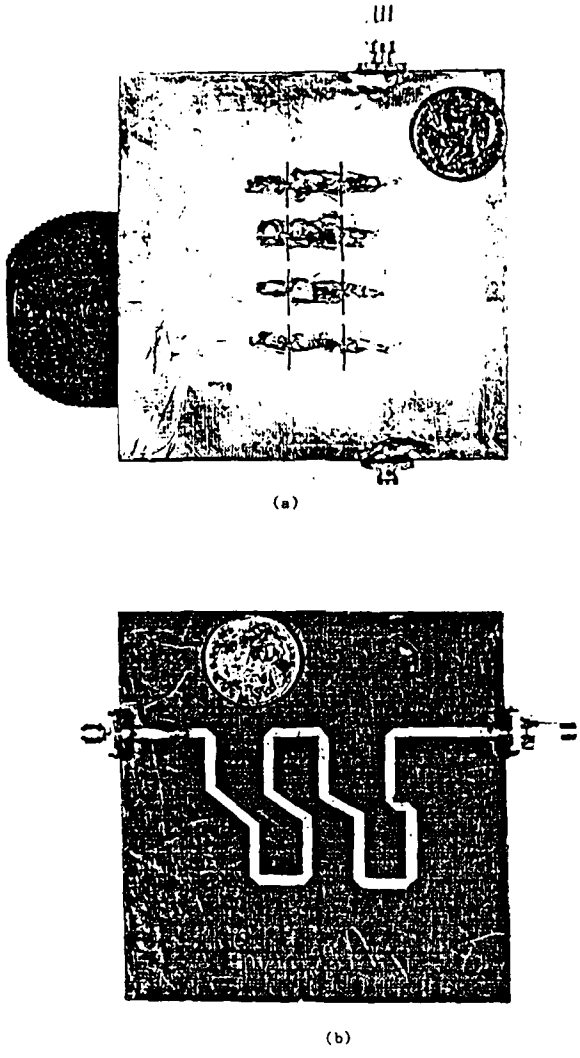


Fig.7. Microstrip Fed Quasi-Optical Frequency Doubling Combiner

3.3 Coupled Slot Antenna

The radiation characteristics of a pair of half wave slot antennas have been studied both theoretically and experimentally. This project is to confirm that the even mode (coupled slot mode) radiates well while the odd mode (coplanar wavegude mode) does

not. The calculations are based on the spectral domain method to find the fields in the slot as well as in the far field. Experiments of the radiation patterns agreed well with the theoretical prediction [13].

### 3.4 Self-Oscillating HEMT Quasi-Optical Mixer

Based on the even and odd mode properties of a coupled slot, a self oscillating, quasi-optical mixer has been designed and built with two HEMT devices at the X band. The coupled slot receives an incoming RF signal in its even mode. One HEMT is placed in each slot and generates a local oscillator signal which is supported by the odd mode in a coupled slot. The RF and LO signals are then mixed in the HEMT devices and down converted to an IF signal which is extracted by a microstrip line on the substrate. An isotropic conversion gain of 5 dB has been attained [14]. Figure 8 shows a schematic of the structure.

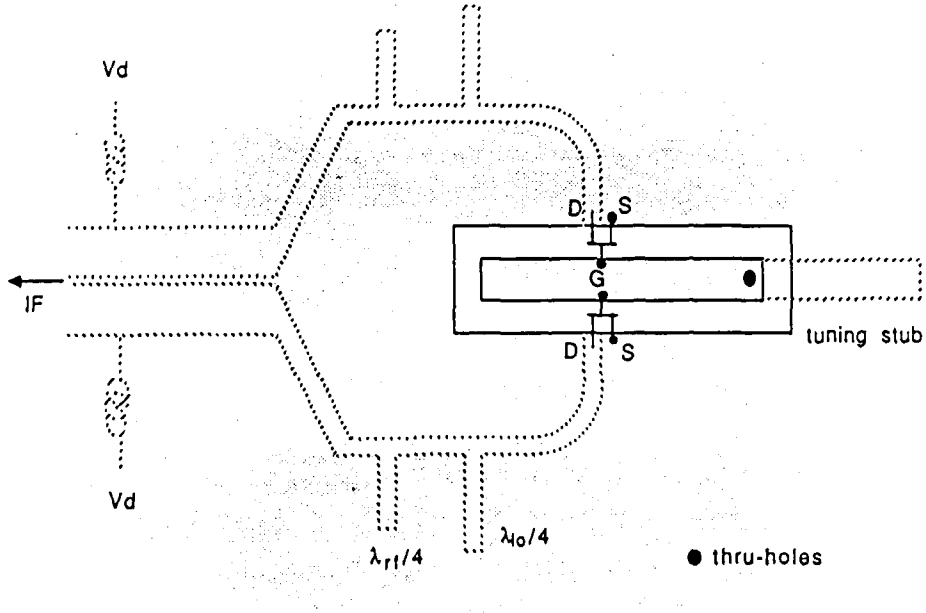


Fig.8 Quasi-optical HEMT self oscillating mixer

## 4. Device Modeling and Characterizations

At higher millimeter-wave frequencies, the width effect of the three terminal devices such as MESFET's can be significant. This effect may be detrimental in a usual device. However, several possibilities exist for using the width effect to create a distributed device in which the guided wave is amplified while it is traveling in the width direction of the device. Before such a device is investigated, it is necessary to characterize conventional three terminal devices both from the device simulation point of view and from the circuit application point of view.

### 4.1 Large Signal Model of GaAs MESFET

An efficient numerical algorithm has been developed for a large signal lumped circuit model of the GaAs MESFET which will aid circuit design and will find the two port charactersitics of the device. The method is base on the conventional hybrid time-frequency domain iterative method called the "multiple reflection technique." However, the convergence has been improved significantly by incorporating an acceleration algorithm similar to the successive under-relaxation technique. The predicted results for a MESFET power amplifier agree well with the measured data [15].

### 4.2 Two-Dimensional Simulation of FET Structures

FET's of several different types have been simulated by means of a finite difference algorithm. The primary purpose of this work is to select a candidate for a traveling wave FET. The simulation program takes into account the energy momentum relations so that the method can simulate FET's with a submicron gate length [16]. Among these structures investigated, an FET with an inverted gate configuration has been selected for the traveling wave device (see Fig. 9). In this configuration, the gate is located on the underside of the active layer through the substrate. The source and the drain are located on the upper side of the active layer in the usual manner. The device should be operated

with a grounded gate mode. Then the source and the drain can be treated in a coupled strip transmission line under the traveling mode of operation. Electrical characteristics of the device have been obtained which will be used in modeling the traveling wave device in work which will be done under the subsequent contract.

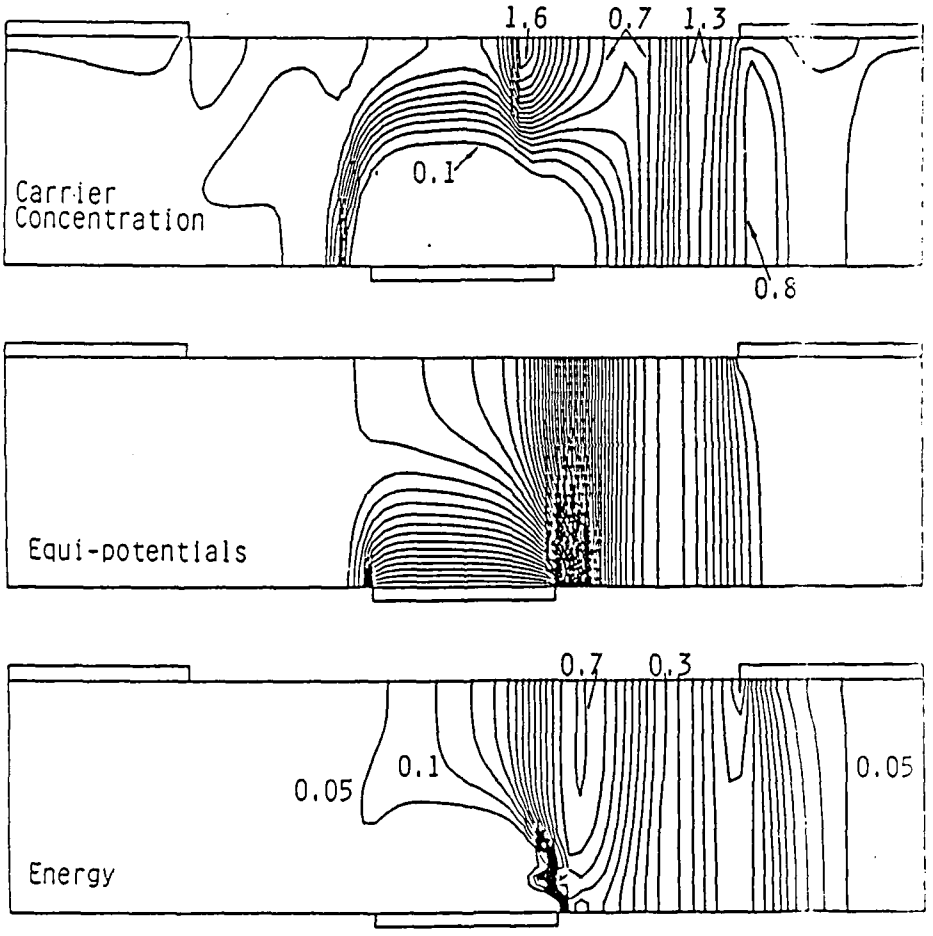


Fig. 9. Carrier Concentration, Potential and Energy Distributions in an Inverted Gate FET

## 5. Slow Wave Structures

One of the problems facing the implementation of millimeter-wave monolithic integrated circuits is the large size of passive devices. They occupy valuable real estate on the GaAs substrate. To alleviate this problem we have done extensive studies on the slow wave structures. Two types of slow wave structures are available. One of them is based on the lossy layer in a semiconductor substrate and another makes use of crosstie metal configuration. The latter one is proposed for extensive study in the subsequent contract. Only very preliminary work was done on this during the report period.

### 5.1 Slow-Wave Coupled Line Structures

The slow wave propagates in a printed transmission line in which the conductors are placed on a thin lossless layer. This is in turn placed on a lossy layer which is created on a lossless substrate (see Fig. 10). *The cause of the slow wave is spatial separation of* the electric energy and the magnetic energy. The electric energy is mainly concentrated in the thin lossless layer while the magnetic field penetrates into the lossy layer and into the substrate beneath. This field separation can be made by an appropriate choice of the structural and material parameters.

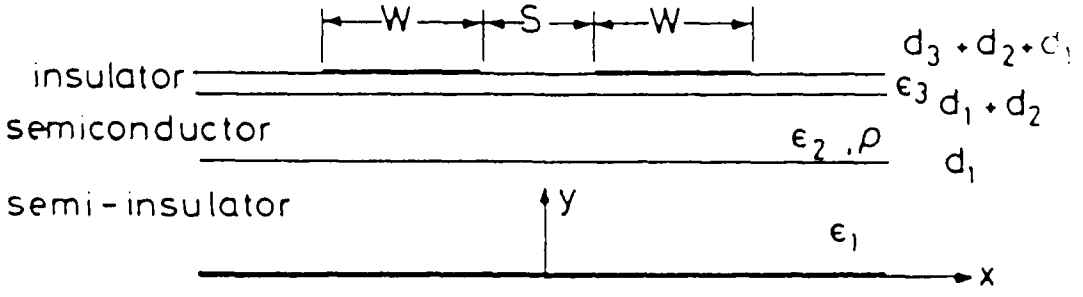


Fig.10 Cross Section of a Slow Wave Structure

The slow wave propagation in a coupled line can be controlled by a number of material and structural parameters. We have discovered that the phase velocities of the even and odd modes can be equalized by a proper choice of these parameters. Hence, it is possible to build a directional coupler with very small physical dimensions. This feature is attractive for GaAs monolithic integrated circuits where the substrate real estate is expensive. A computer program has been developed for design of directional couplers both in the forward and backward waves [17].

## 5.2 Crosstie CPW and Microstrip Slow Wave Structures

A new slow wave structure which does not depend on the substrate loss has been conceived. The structure is either a coplanar waveguide (CPW) or a microstrip line on which a thin dielectric overlay is placed. Periodic crosstie strips oriented in the transverse direction are placed on the overlay. The schematic is shown in Fig. 11. The capacitance between the crosstie and the center strip of the microstrip or the center strip of the CPWcan be made extremely large. Since the structure is now a cascaded chain of capacitive and inductive sections, the electric and magnetic energy are spatially separated to cause a slow wave effect. It is important that the operating wavelength be sufficiently longer than one period of the crosstie CPW or microstip line so that the structure simulates a uniform transmission line. Due to a large capacitance and inductance per unit length, the phase velocity is extremely small and hence the slow wave is obtained. A preliminary calculation suggests that a slow wave factor of more than 10 can be obtained [18]. There are a number of conceivable interesting applications. They include a bandstop filter made of a doubly periodic grating and other types of filters. All of them are expected to be small in size. These devices will be investigated in the subsequent contract period.

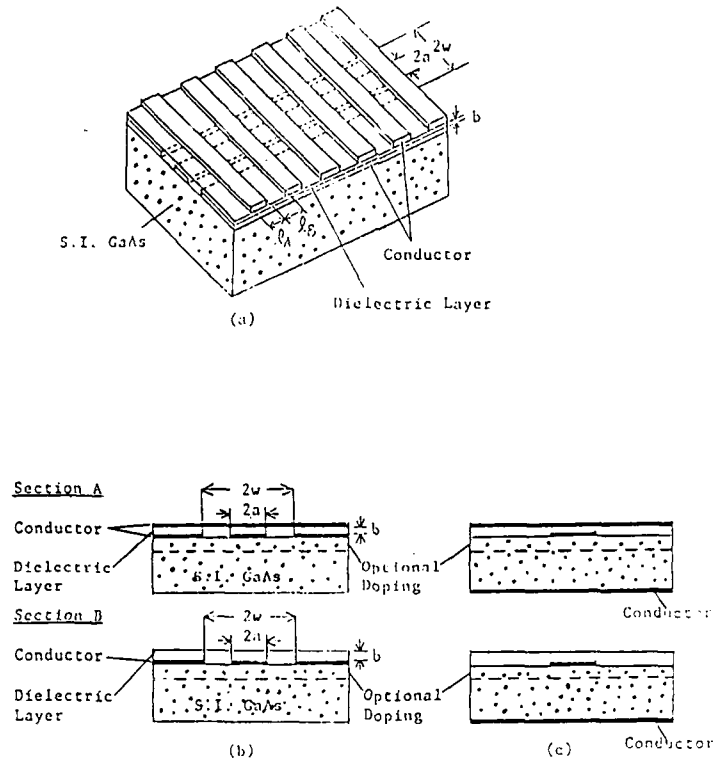


Fig.11. Crosstie Slow Wave Structrures

## 6. Broadband Planar Optical Modulator

The major limitation of a traveling wave optical modulator is velocity matching between the guided optical wave and the modulating microwave signal. A mismatch of the phase velocity between these two waves limit the bandwidth of the modulator. The optical wave is guided typically by a waveguide which is buried in a substrate material. On the other hand, the microwave signal propagates along a strip conductor on the surface of the substrate. In the case of a GaAs based modulator, the phase velocities of the microwave signal is much faster. Since the new crosstie overlay coplanar waveguide described in the previous section has the capability of slowing down the microwave signal, this structure can be used as the propagation path of the modulating microwave signal for a traveling wave integrated optical modulator created with a GaAs material.

Another important parameter of the traveling wave modulator is the charactersitics impedance of the microwave signal path. The crosstie structure has the capability of adjusting the characteristic impedance in addition to the phase velocity. It is possible to attain a broadband impedance matching by this structure.

The crosstie structure is provided via a dielectric overlay on a coplanar waveguide electrode which is placed on a GaAs/GaAlAs layered structure. The optical waveguide is in the form of a GaAs channel waveguide (see Fig. 12). A preliminary investigation leading to the design of this optical modulator is reported in [19] (see Appendix 4).

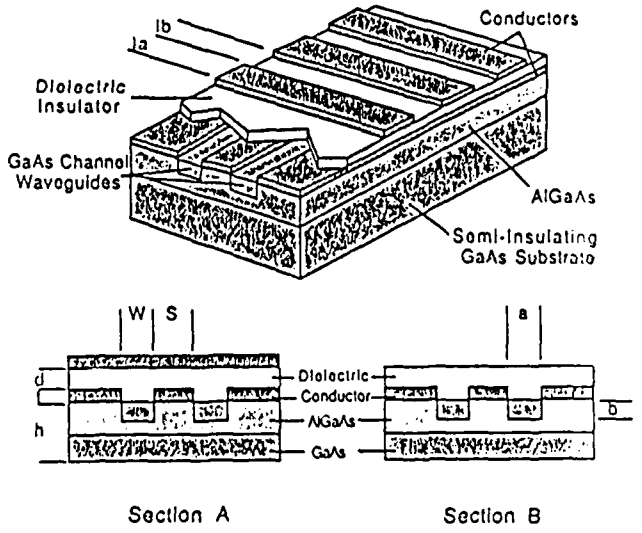


Fig.12. Crosstie CPW Traveling Wave Optical Modulator

## References


1. T. S. Chu, T. Itoh and Y. Shih, "Comparative study of mode-matching formulations for microstrip discontinuity problems," IEEE Trans. Microwave Theory and Tech., Vol. MTT-33, No.10, pp. 1018-1023, October 1985.

2. T. S. Chu and T. Itoh, "Analysis of microstrip step discontinuity by the modified residue calculus technique," IEEE Trans. Microwave Theory and Tech., Vol. MTT-33, No. 10, pp. 1024-1028, October 1985.

3. T. S. Chu and T. Itoh, "Generalized scattering matrix method for analysis of cascaded and offset microstrip step discontinuities," IEEE Trans. Microwave Theory and Tech., Vol. MTT-34, No. 2, pp. 280-284, February 1986.

4. Q. Zhang and T. Itoh, "Analysis of waveguide scattering problems by the spectral domain method," Electronics Letters, Vol. 22, No. 15, pp. 822-823, July 17, 1986.

5. Q. Zhang and T. Itoh, "Spectral domain analysis of scattering from E-plane circuit elements," IEEE Trans. Microwave Theory and Tech., Vol. MTT-35, No. 2, pp. 138-150, February 1987.

6. Q. Zhang and T. Itoh, "Computer-aided design of evanescent mode waveguide filter with non-touching E-plane fins," IEEE Trans. Microwave Theory and Tech., Vol. 36, No. 2, pp. 404-412, February 1988.

7. M. Geshiro and T. Itoh, "Analysis of double-layered finlines containing a magnetized ferrite," IEEE Trans. Microwave Theory and Tech., Vol. MTT-35, No. 12, pp. 1377-1381, December 1987.

8. B. Young and T. Itoh, "Loss reduction in superconducting microstrip-like transmission lines," 1988 IEEE MTT-S International Microwave Symposium, May 25-27, 1988, New York, NY.

9 K. D. Stephan, N. Camilleri and T. Itoh, "A quasi-optical polarization-duplexed mixer for millimeter-wave applications," IEEE Trans. Microwave Theory and Tech., Vol. MTT-31, No. 2, pp. 164-170, February 1983.

10. K. D. Stephan and T. Itoh, "A planar quasi-optical subharmonic mixer characterized by isotropic conversion loss," IEEE Trans. Microwave Theory and Tech., Vol. MTT-32, No. 1, pp. 97-102, January 1984.

11. N. Camilleri and T. Itoh, "A quasi-optical multiplying slot array," IEEE Trans. Microwave Theory and Tech., Vol. MTT-33, No. 11, pp. 1189-1195, November 1985.

12. S. Nam, T. Uwano and T. Itoh, "Microstrip fed planar frequency-multiplying space combiner," IEEE Trans. Microwave Theory and Tech., Vol. MTT-35, No. 12, pp. 1271-1276, December 1987.

13. T. H. Wang, T. Itoh and H. Ling, "Spectral domain analysis of a coupled slot antenna," IEEE Trans. Antennas and Propagation, Vol. 36, 1988.

14. V. D. Hwang and T. Itoh, "A quasi-optical HEMT self oscillating mixer," 1988 IEEE MTT International Microwave Symposium, May 25-27, 1988, New York, NY.

15. V. D. Hwang and T. Itoh, "An efficient approach for large signal modeling and analysis of the GaAs MESFET," IEEE Trans. Microwave Theory and Tech., Vol. MTT-35, No. 4, pp. 396-401, April 1987.

16. S. El-Ghazaly and T. Itoh, "Inverted-gate field-effect transistors; Novel high frequency structures, " submitted to IEEE Trans. Electron Devices.

17. H. Ogawa and T. Itoh, "Slow-wave directional coupler and its application," International J. Infrared and Millimeter Waves, Vol. 7, No. 10, pp.1417-1427, October 1986.

18. T. H. Wang and T.Itoh, "Compact grating structure for application to filters and resonators in monolithic microwave integrated circuits," IEEE Trans. Microwave Theory and Tech., Vol. MTT-35, No. 12, pp. 1176-1182, December 1987.

19. H.-Y. Lee, T.-H. Wang and T. Itoh, "Crosstie overlay slow-wave structures for broadband electro-optical traveling-wave modulator," International J. Infrared and Millimeter Waves, Vol. 9, No. 1, January 1988.

**List of Personnel**

Principal Investigator
T. Itoh

Faculty Associate
D. P. Neikirk

Research Associate
H. Ogawa
Y. Nikawa
Q. Zhang

Visiting Scholar
P. Ray
T. Uwano
M. Geshiro

Research Assistant / Students
N. Camilleri
Q. Zhang
T. S. Chu
T. C. Mu
V. D. Hwang
B. Fazio
S. Nam
T. H. Wang
S. El-Ghazaly
H. Y. Lee
B. Young
S. S. Chang

**Degrees Awarded**

| | | |
|---|---|---|
| Master of Science | T. S. Chu | May 1985 |
| | T. C. Mu | Dec. 1985 |
| | V. D. Hwang | May 1986 |
| Ph.D. | N. Camilleri | May 1985 |
| | Q. Zhang | May 1987 |
| | B. Young | Dec. 1987 |

## Journal Publications Under ARO Support (Oct. 1984 - to date)


1. "Inexpensive short-range microwave telemetry transponder," Electronics Letters, Vol. 20, No. 21, pp. 877-878, October 11, 1984, (K. D. Stephan and T. Itoh).

2. "Transverse resonance analysis of finline discontinuities," IEEE Trans. Microwave Theory and Techniques, Vol. MTT-32, No. 12, pp. 1633-1638, December 1984, (R. Sorrentino and T. Itoh).

3. "Broadband Millimeter-wave E-plane bandpass filters," IEEE Trans. Microwave Theory and Techniques, Vol. MTT-32, No. 12, pp. 1655-1658, December 1984, (L.Q. Bui, D. Ball and T. Itoh).

4. "Field analysis of a millimeter-wave GaAs double-drift IMPATT diode in the traveling-wave mode," IEEE Trans. Microwave Theory and Techniques, Vol. MTT-33, No. 3, pp. 216-221, March 1985, (Y. Fukuoka and T. Itoh).

5. "Modified residue calculus technique for microstrip step discontinuities," Electronics Letters, Vol. 21, No. 7, pp. 257-258, March 28, 1985, (T.S. Chu and T. Itoh).

6. "Analysis of multilayer interconnection lines for a high speed digital integrated circuit," IEEE Trans. Microwave Theory and Techniques, Vol.MTT-33, No. 6, pp. 527-532, June 1985, (Y. Fukuoka, Q. Zhang, D.P. Neikirk and T. Itoh).

7. "Analysis of a suspended patch antenna excited by an electromagnetically coupled inverted microstrip feed," IEEE Trans. Antennas and Propagation, Vol. AP-33, No. 8, pp.895-899, August 1985, (Q. Zhang, Y. Fukuoka and T. Itoh).

8. "Characteristics of coupled slow-wave microstrip lines," Electronics Letters, Vol.21, No. 20, pp.946-947, Sept. 26, 1985, (T.C. Mu, H. Ogawa and T. Itoh).

9. "Comparative study of mode-matching formulations for microstrip discontinuity problems," IEEE Trans. Microwave Theory and Techniques, Vol.MTT-33, No. 10, pp.1018-1023, October 1985, (T.S. Chu, T. Itoh and Y.C. Shih).

10. "Analysis of microstrip step discontinuity by the modified residue calculus technique," IEEE Trans. Microwave Theory and Techniques, Vol.MTT-33, No. 10, pp.1024-1028, October 1985, (T.S. Chu and T. Itoh).

11. "A quasi-optical multiplying slot array," IEEE Trans. Microwave Theory and Techniques, Vol. MTT-33, No. 11, pp. 1189-1195, November 1985, (N. Camilleri and T. Itoh).

12. "Generalized scattering matrix method for analysis of cascaded and offset microstrip step discontinuities," IEEE Trans. Microwave Theory and Techniques, Vol.MTT-34, No. 2, pp.280-284, Feb. 1986, (T.S. Chu and T. Itoh).

13. "Slow-wave Power Divider," Electronics Letters, Vol. 22, No. 13, pp. 692-693, June 19, 1986 (H. Ogawa and T. Itoh).

14. "Analysis of Waveguide Scattering Problems by the Spectral Domain Method," Electronics Letters, Vol. 22, No. 15, pp. 822-823, July 17, 1986 (Q. Zhang and T. Itoh).

15. "An overview on numerical techniques for modeling miniaturized passive components," Annales des Telecommunications, Vol. 41, No.9-10, pp. 449-462, Sept.- Oct., 1986.

16. "Slow-wave Directional Coupler and Its Application," International J. Infrared and Millimeter Waves, Vol. 7, No. 10, pp. 1417-1427, Oct. 1986 (H. Ogawa and T. Itoh).

17. "Characteristics of Multiconductor, Asymmetric, Slow-wave Microstrip Transmission Lines," IEEE Trans. Microwave Theory and Techniques, Vol. MTT-34, No. 12, pp. 1471-1477, December 1986 (T. C. Mu, H. Ogawa and T. Itoh).

18. "Slow-Wave Characteristics of Ferromagnetic Semiconductor Microstrip Line," IEEE Trans. Microwave Theory and Techniques, Vol. MTT-34, No. 12, pp. 1478-1482, December 1986 (H. Ogawa and T. Itoh).

19. "Spectral Domain Analysis of Scattering from E-plane Circuit Elements," IEEE Trans. Microwave Theory and Techniques, Vol. MTT-35, No. 2, pp. 138-150, February 1987 (Q. Zhang and T. Itoh).

20. "An Efficient Approach for Large Signal Modeling and Analysis of the GaAs MESFET," IEEE Trans. Microwave Theory and Techniques, Vol. MTT-35, No. 4, pp. 396-401, April 1987 (V.D. Hwang and T. Itoh).

21. "Microstrip Fed Planar Frequency-Multiplying Space Combiner," IEEE Trans. Microwave Theory and Techniques, Vol. MTT-35, No. 12, pp. 1271-1276, December 1987 (S. Nam, T. Uwano and T. Itoh).

22. "Analysis of Double-Layered Finlines Containing a Magnetized Ferrite," IEEE Trans. Microwave Theory and Techniques, Vol. MTT-35, No. 12, pp. 1377-1381, December 1987, (M. Geshiro and T. Itoh).

23. "Compact Grating Structure for Application to Filters and Resonators in Monolithic Microwave Integrated Circuits," IEEE Trans. Microwave Theory and Techniques, Vol. MTT-35, No. 12, pp. 1176-1182, December 1987 (T. H. Wang and T. Itoh).

24. "Complex Modes in Lossless Shielded Microstrip Lines," IEEE Trans. Microwave Theory and Techniques, Vol. MTT-36, No. 1, January 1988 (W. -X. Huang and T. Itoh).

25. "Computer-Aided Design of Evanescent Mode Waveguide Filter with Non-Touching E-Plane Fins," IEEE Trans. Microwave Theory and Techniques (Special Issue on Computer-Aided Design), Vol. MTT-36, No. 2, February 1988 (Q. Zhang and T. Itoh).

26. "Spectral Domain Analysis of a Coupled Slot Antenna," IEEE Trans. Antennas and Propagation, (T. H. Wang, T. Itoh and H. Ling).

27. "Two-Dimensional Numerical Simulation of Short-Gate-Length GaAs MESFET's and Application to Study the Traveling Gunn Domain Phenomena," Int. J. of Numerical Modeling, Vol. 1, (S. El-Ghazaly and T. Itoh).

28. "Crosstie Overlay Slow-Wave Structures for Broad-Band Electro-Optical Traveling-Wave Modulators," Int. J. Infrared and MM Waves, (H. -Y. Lee, T.-H. Wang and T. Itoh).

**Conference Publications under ARO Support (July 84 - to date)**

1. "Fin-line and E-plane structures for millimeter wave circuits," XXIst General Assembly of URSI Digest, P. 434, August 28-September 5, 1984, Florence, Italy, (T. Itoh).

2. "Analysis of a suspended patch antenna excited by an electromagnetically coupled inverted microstrip feed," 14th European Microwave Conference Proceedings, pp. 613-618, September 10-13, 1984, Liege, Belgium, (Q. Zhang, Y. Fukuoka, T. Itoh and L. Su).

3. "Travelling-wave characteristics of millimeter-wave IMPATT diode," 9th International Conf. on Infrared and Millimeter Waves Digest, p. 528, October 22-26, 1984, Takarazuka, Japan, (Y. Fukuoka and T. Itoh).

4. "Survey of millimeter-wave guiding structures," SPIE Technical Symposium East '85, April 8-12, 1985, Arlington, VA, (T. Itoh).

5. "Comparative study of mode matching formulations for microstrip discontinuity problems," 1985 IEEE MTT-S International Microwave Symposium Digest, pp. 435-438, June 4-6, 1985, St. Louis, MO, (Y.C. Shih, T.S. Chu and T. Itoh).

6. "New waveguide structures for microwave and millimeter circuits," 1985 International Symposium on Microwave Technology in Industrial Development-Brazil, pp. 205-208, July 22-25, 1985, Campinas, Brazil, (T. Itoh).

7. "Frequency multiplying active slot array," Proc. of 1985 International Symposium on Antennas and Propagation, pp. 739-742, August 20-22, 1985, Kyoto, Japan, (N. Camilleri and T. Itoh).

8. "An overview on numerical techniques for modeling miniaturized passive components," (Invited) 15th European Microwave Conference, pp. 1059-1063, September 9-12, 1985, Paris, France, (T. Itoh).

9. "Analysis of offset microstrip step discontinuity by the generalized scattering matrix techniques," 15th European Microwave Conference, pp. 814-819, September 9-12, 1985, Paris, France, (T.S. Chu and T. Itoh).

10. "Frequency multiplying power-combining slot array," 15th European Microwave Conference, pp. 194-197, September 9-12, 1985, Paris, France, (N. Camilleri and T. Itoh).

11. "Comparative study of millimeter-wave guided structures," (Invited) 10th Internatinal Conference on Infrared and Millimeter Waves Digest, pp. 232-233, December 9-13, 1985, Lake Buena Vista, FL, (T. Itoh).

12. "Slow-wave characteristics of ferromagnetic semiconductor microstrip transmission lines," 1986 IEEE MTT-S International Microwave Symposium Digest, pp. 65-68, June 2-4, 1986, Baltimore, MD, (H. Ogawa and T. Itoh).

13. "Characteristics of milticonductor, asymmetric, slow-wave microstrip transmission lines," 1986 IEEE MTT-S International Microwave Symposium Digest, pp. 695-698, June 2-4, 1986, Baltimore, MD, (T.C. Mu, H. Ogawa and T. Itoh).

14. "An overview of numerical techniques for microwave and millimeter- wave passive components," URSI International Symposium on Electromagnetic Theory, pp. 174-175, August 25-29, 1986, Budapest, Hungary, (T. Itoh).

15. "Large Signal Modelling and Analysis of GaAs MESFET," 16th European Microwave Conference, pp. 189-194, Sept. 8-12, 1986, Dublin, Ireland (V. D. Hwang and T. Itoh).

16. "Design Consideration of Coupled Slow-wave Microstrip-line Circuits," 16th European Microwave Conference, pp. 477-482, Sept. 8-12, 1986, Dublin, Ireland (H. Ogawa and T. Itoh).

17. "Coupled Slow-wave Microstrip Line MMIC's," 11th International Conference on Infrared and Millimeter Waves," pp. 174-176, Oct. 20-24, 1986, Pisa, Italy (H. Ogawa and T. Itoh).

18. "Recent Advances in Quasi-Optical Planar Structures" (Invited), Melecon '87, pp. 331-332, March 24-26, 1987, Rome, Italy (T. Itoh).

19. "Compact Grating Structure for Applications to Filters and Resonators for Monolithic Microwave Integrated Circuits," 1987 IEEE MTT-S International Microwave Symposium Digest, pp. 315-318, Las Vegas, NV, June 9-11, 1987 (T. H. Wang and T. Itoh).

20. "Analysis of a Double-Layered Finline Containing a Magnetized Ferrite," 1987 IEEE MTT-S International Microwave Symposium Digest, pp. 743-744, Las Vegas, NV, June 9-11, 1987 (M. Geshiro and T. Itoh).

21. "Microstrip Fed Planar Frequency multiplying Space Combiner," 1987 IEEE MTT-S International Microwave Symposium Digest, pp. 945-948, Las Vegas, NV, June 9-11, 1987 (S. Nam, T. Uwano and T. Itoh).

22. "Spectral Domain Analysis of a Coupled Slot Antenna," 1987 IEEE Antennas and Propagation Society International Symposium Digest, pp. 1182-1185, Blacksburg, VA, June 15-19, 1987 (T. H. Wang, T. Itoh and H. Ling).

23. "Experimental Design of Frequency Multiplying Slot Array Antenna Fed by Microstrip," 1987 IEEE Antennas and Propagation Society International Symposium Digest, pp. 1186-1189, Blacksburg, VA, June 15-19, 1987 (S. Nam, T. Uwano and T. Itoh).

24. "Overview of Numerical Methods for Characterization of Millimeter-Wave Passive Integrated Structures," (Invited) 1987 International Microwave Symposium/Brazil, pp. 387-392, Rio de Janerio, Brazil, July 27-30, 1987 (T. Itoh).

25. "Effect of Electron Injection into MESFET substrates," 22nd General Assembly of the International Union of Radio Science, Tel Aviv, Israel, p. 7, August 24 - Sept. 2, 1987 (S. El-Ghazaly and T. Itoh).

26. "Inverted-Gate GaAs MESFET Characteristics," 17th European Microwave Conference, pp. 113-118, Sept. 7-11, 1987, Rome, Italy (S. El-Ghazaly and T. Itoh).

27. "Analysis and Design of Evanescent Mode Waveguide Filter with Non-Touching E-Plane Fins," 17th European Microwave Conference, pp. 1032-1037, Sept. 7-11, 1987, Rome, Italy (Q. Zhang and T. Itoh).

28. "Crosstie Overlay Slow-Wave Structure for Broad-Band Traveling-Wave Electrooptical Modulators", 12th International Conference on Infrared and Millimeter Waves, Dec. 14-18, 1987, Lake Buena Vista, FL (H. Y. Lee, T. H. Wang and T. Itoh).

**Technical Reports**

1. "A multiplying slot array," Electrical Engineering Research Laboratory Report, No. 85-P-1, University of Texas, May 1985, (N. Camilleri and T. Itoh).

2. "Analysis of microstrip discontinuities," Electrical Engineering Research Laboratory Report, No.85-P-2, University of Texas, May 1985, (T.S. Chu and T. Itoh).

3. "Large signal modeling and analysis of GaAs MESFET," Electrical Engineering Research Laboratory Report No.86-P-2, June 1986, (V. Hwang and T. Itoh).

4. "A Study of Scattering from E-plane Circuit Elements," Microwave Laboratory Report No. 87-P-5, May 1987, (Q. Zhang and T. Itoh).

# APPENDIX 1

# Comparative Study of Mode-Matching Formulations for Microstrip Discontinuity Problems

TAK SUM CHU, TATSUO ITOH, FELLOW, IEEE, AND YI-CHI SHIH, MEMBER, IEEE

*Abstract*—**Several matrix formulations for the microstrip step-discontinuity problem are compared. Although they are theoretically identical, one of them has an advantage in numerical labor, relative, and absolute convergence. Results of this method are checked with other published data and with those independently obtained by the modified residue calculus technique.**

## I. Introduction

A STEP DISCONTINUITY is frequently encountered in microstrip line circuits and, hence, its analysis is important for circuit design. There are several approaches available. When the microstrip is enclosed in a waveguide-like case, it is possible to calculate the fundamental and higher order modes in both sides of the step and to impose the continuity conditions of the tangential field in the cross section of the shield case at the step location. This process leads to a system of mode-matching equations. When an open microstrip line circuit is dealt with, the higher order modes can become radiation modes which must be included in the mode-matching procedure.

In many applications, the so-called waveguide model has been found useful for calculation of the scattering at the microstrip discontinuity [1]–[3]. In this paper, we assume that the waveguide model is an acceptable technique for the calculation of the step-continuity problem. In addition, radiation and surface waves are not considered. The motivation for the present work is somewhat different from those published. Although a number of numerical data are presented in the literature [1]–[3], details of the numerical process are not clear. The objective of the present paper is not to duplicate the numerical data already available, but to place some foundation on how these data should be calculated. We present several alternative formulations. Although these formulations are theoretically identical, it is pointed out that the numerical labor and accuracy depend on the choice of formulation and some are better than others.

Manuscript received February 4, 1985; revised May 14, 1985. This work was supported in part by the U.S. Army Research Office under Contract DAAG 29-84-k-0076.

T. S. Chu and T. Itoh are with the Department of Electrical and Computer Engineering, University of Texas, Austin, TX 78712.

Y-C. Shih is with Hughes Aircraft Company, Microwave Products Division, Torrance, CA 90509.


Fig. 1. The waveguide model of the open microstrip line.

The best formulation can be decided based on the matrix size, relative and absolute convergence, and other numerical considerations. It turns out that the best formulation is the one we often choose without clear reasoning. The data for a microstrip step discontinuity are compared with available data. They are also compared with the modified residue calculus technique, which serves as an independent check of the numerical accuracy.

Before starting the formulation, let us briefly review the waveguide model. In this technique, the uniform microstrip line of width $w_0$ on the substrate of height $h$ and relative dielectric constant $\epsilon_r$ is replaced with an equivalent parallel-plate waveguide with magnetic side walls (Fig. 1). The substrate height is kept identical. However, the effective width $w_{eff}$ and the effective dielectric constant $\epsilon_{eff}$ are used to define the effective waveguide in such a way that the effect of the fringing field of the microstrip is taken into account. Specifically, these effective values are related to the propagation constant $\beta$ and the characteristic impedance $Z_0$ via

$$\epsilon_{eff} = (\beta/k_0)^2$$

$$Z_0 = \left(120\pi/\sqrt{\epsilon_{eff}}\right)(h/w_{eff}). \tag{1}$$

Note that $\beta$ and $Z_0$ can be found from a standard analysis such as the spectral-domain method, from curve fitting, or an empirical formula, once the structural parameters of the microstrip line are given.

For the analysis of the step discontinuity, both sides of the step are replaced with their respective equivalent waveguides. Note that the heights of these two waveguides are identical. Hence, the problem remains a two-dimensional one as the field is uniform in the $y$- (vertical) direction. Also, note that the dominant mode in the equivalent waveguide is TEM. In the following sections, all structural parameters used, except $h$, are presumed to be the "effective" ones, unless otherwise stated.

0018-9480/85/1000-1018$01.00 ©1985 IEEE

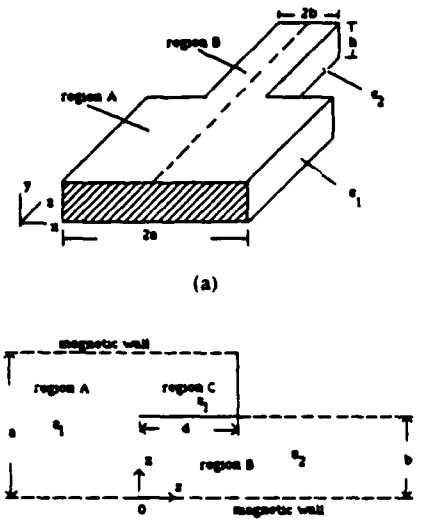


Fig. 2. (a) Waveguide model for symmetric microstrip step discontinuity. (b) Auxiliary geometry for the waveguide problem.

## II. Formulation

The problem under study is the waveguide model for the microstrip step discontinuity shown in Fig. 2(a). The structure is assumed to be symmetrical, and the parallel-plate waveguide is idealized with magnetic side walls. For convenience of analysis, an auxiliary structure is introduced in Fig. 2(b). Only one half of the original structure is considered because of symmetry, and the transversal magnetic wall at the discontinuity is recessed to create a new region C. The original structure is recovered by letting $d = 0$.

The mode-matching procedure begins by expanding the tangential electric and magnetic fields at the junction in terms of the normal modes on both sides of the junction. For $TE_{n0}$ $(n = 0, 1, \cdots)$ excitation, we write down the $E_y$ continuity equation

$$\sum_{n=0}^{M-1} (A_n^+ + A_n^-)\phi_{an} = \begin{cases} \sum_{n=0}^{K-1} (B_n^+ + B_n^-)\phi_{bn}, & 0 \le x \le 0 \\ \sum_{n=0}^{L-1} C_n \phi_{cn}(1+\rho_n), & b \le x \le a \end{cases} \tag{2a}$$

and a corresponding one for $H_x$

$$\sum_{n=0}^{M-1} (A_n^+ - A_n^-) Y_{an}\phi_{an} = \sum_{n=0}^{K-1} (B_n^+ - B_n^-) Y_{bn}\phi_{bn}, \quad 0 \le x \le b$$

$$= \sum_{n=0}^{L-1} C_n Y_{cn}\phi_{cn}(1-\rho_n), \quad b \le x \le a \tag{2b}$$

where

$$\phi_{an} = \sqrt{(\epsilon_{n0}/a)}\cos(k_{an}x), \qquad k_{an} = (n\pi/a)$$
$$\phi_{bn} = \sqrt{(\epsilon_{n0}/b)}\cos(k_{bn}x), \qquad k_{bn} = (n\pi/b)$$
$$\phi_{cn} = \sqrt{(\epsilon_{n0}/c)}\cos(k_{cn}(a-x)), \qquad k_{cn} = (n\pi/c)$$
$$\epsilon_{n0} = \begin{cases} 1, & n = 0 \\ 2, & n \ne 0 \end{cases}$$

and

$$Y_{an} = \sqrt{\left(\epsilon_1 k_0^2 - (n\pi/a)^2\right)} = \beta_n$$
$$Y_{bn} = \sqrt{\left(\epsilon_2 k_0^2 - (n\pi/b)^2\right)} = \gamma_n$$
$$Y_{cn} = \sqrt{\left(\epsilon_1 k_0^2 - (n\pi/c)^2\right)} = \bar{\beta}_n$$
$$\rho_n = \exp(-2j\bar{\beta}_n d).$$

In (2), $\phi_{an}$, $\phi_{bn}$, and $\phi_{cn}$ are normal modes in Regions A, B, and C, with propagation constants $\beta_n$, $\gamma_n$, and $\bar{\beta}_n$, respectively. $A_n^+$ and $B_n^-$ are the given incident field coefficients from Regions A and B (usually only one $A_n^+$ or $B_n^-$ is considered at a time), while $A_n^-$, $B_n^+$, and $C_n$ are the unknown excited field coefficients in regions A, B, and C, respectively. $\rho_n$ is the reflection from the magnetic wall in Region C.

From modal orthogonality, we obtain the linear simultaneous equations for the unknown modal coefficients

$$A_m^+ + A_m^- = \sum_{n=0}^{K-1} H_{mn}(B_n^+ + B_n^-) + \sum_{n=0}^{L-1} \bar{H}_{mn} C_n (1+\rho_n)$$

$$Y_{am}(A_m^+ - A_m^-) = \sum_{n=0}^{K-1} H_{mn} Y_{bn}(B_n^+ - B_n^-) + \sum_{n=0}^{L-1} H_{mn} Y_{cn} C_n (1-\rho_n),$$
$$m = 0, 1, 2, \cdots, M-1 \tag{3a}$$

$$\sum_{n=0}^{M-1} H_{nm}(A_n^+ + A_n^-) = B_m^+ + B_m^-$$

$$\sum_{n=0}^{M-1} H_{nm} Y_{an}(A_n^+ - A_n^-) = Y_{bm}(B_m^+ - B_m^-),$$
$$m = 0, 1, 2, \cdots, K-1 \tag{3b}$$

$$\sum_{n=0}^{M-1} \bar{H}_{nm}(A_n^+ + A_n^-) = C_m(1+\rho_m)$$

$$\sum_{n=0}^{M-1} \bar{H}_{nm} Y_{an}(A_n^+ - A_n^-) = C_m Y_{cm}(1-\rho_m),$$
$$m = 0, 1, 2, \cdots, L-1 \tag{3c}$$

where

$$H_{mn} = \int_0^b \phi_{am}\phi_{bn}\, dx = \left(\frac{\epsilon_{m0}\epsilon_{n0}}{ab}\right)^{1/2}\left(\frac{1}{2}\right)\left(\frac{2k_{am}(-1)^n \sin(k_{am}b)}{k_{am}^2 - k_{bn}^2}\right)$$

$$\bar{H}_{mn} = \int_b^a \phi_{am}\phi_{cn}\, dx = \left(\frac{\epsilon_{m0}\epsilon_{n0}}{ac}\right)^{1/2}\left(\frac{1}{2}\right)\left(\frac{2k_{am}(-1)^{n+1} \sin(k_{am}b)}{k_{am}^2 - k_{cn}^2}\right).$$

To condense the above equations, we define the following matrices:

$$Y_i = \begin{bmatrix} Y_{i0} & 0 & \cdots & \\ & Y_{i1} & & \\ 0 & & Y_{i2} & \\ \vdots & & & \ddots \\ & & & Y_{in} \end{bmatrix},$$

$$i = a, b, c$$
$$n = M-1, K-1, L-1,$$

$$R = \begin{bmatrix} 1+\rho_0 & 0 & \cdots & \\ 0 & 1+\rho_1 & & \\ \vdots & & \ddots & \\ & & & 1+\rho_n \end{bmatrix}$$

$$R' = \begin{bmatrix} 1-\rho_0 & 0 & \cdots & \\ & 1-\rho_1 & & \\ 0 & & \ddots & \\ \vdots & & & 1-\rho_n \end{bmatrix}$$

$$n = L-1$$

$$Y_d = \left[\begin{array}{c|c} Y_b & 0 \\ \hline 0 & Y_c \end{array}\right] \quad \bar{R}' = \left[\begin{array}{c|c} I & 0 \\ \hline 0 & R' \end{array}\right] \quad \bar{R} = \left[\begin{array}{c|c} I & 0 \\ \hline 0 & R \end{array}\right]$$

$$G = [\, H \mid \bar{H} \,]$$

where $I$ is the identity matrix, $H$ is a matrix of size $M \times K$ with generic element $H_{mn}$ as defined above, while $\bar{H}$ is a matrix of size $M \times L$ with generic element $\bar{H}_{mn}$.

Then, the mode-matching equations can be written in the following matrix form:

$$\underline{a}^+ + \underline{a}^- = G\bar{R}\underline{d}^+ + G\underline{d}^- \tag{4a}$$

$$Y_a(\underline{a}^+ - \underline{a}^-) = GY_d\bar{R}'\underline{d}^+ - GY_d\underline{d}^- \tag{4b}$$

$$G^T(\underline{a}^+ + \underline{a}^-) = \bar{R}\underline{d}^+ + \underline{d}^- \tag{4c}$$

$$G^TY_a(\underline{a}^+ - \underline{a}^-) = Y_d\bar{R}'\underline{d}^+ - Y_d\underline{d}^- \tag{4d}$$

where superscript $T$ denotes transpose operation, and

$$\underline{a}^+ = \begin{bmatrix} A_0^+ \\ A_1^+ \\ A_2^+ \\ \vdots \\ A_{M-1}^+ \end{bmatrix} \quad \underline{d}^- = \left[\begin{array}{c} B_0^- \\ B_1^- \\ \vdots \\ B_{K-1}^- \\ \hline 0 \\ \vdots \\ 0 \end{array}\right]$$

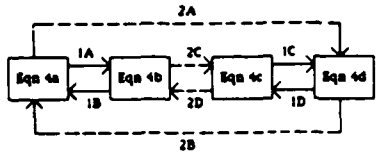


Fig. 3. Classification of formulations.

$$\underline{d}^+ = \left[\begin{array}{c} B_0^+ \\ B_1^+ \\ \vdots \\ B_{K-1}^+ \\ \hline C_0 \\ C_1 \\ \vdots \\ C_{L-1} \end{array}\right] \quad \underline{a}^- = \begin{bmatrix} A_0^- \\ A_1^- \\ A_2^- \\ \vdots \\ A_{M-1}^- \end{bmatrix}$$

$\underline{a}^+$ and $\underline{d}^-$ are column vectors of the excitation terms and $\underline{a}^-$ and $\underline{d}^+$ are column vectors of the unknown modal coefficients. All matrices are of size $(M \times M)$; this requires that $K + L = M$.

When $M \to \infty$, we can prove that $G^{-1} \equiv G^T$. Therefore, (4a) and (4b) are equivalent to (4c) and (4d). Two independent vector equations are required to solve for two unknown vectors. Hence, for four pairs of equations ((4a) and (4b), (4b) and (4c), (4c) and (4d), and (4d) and (4a)), substituting one equation into the other in the same pair, we have eight ways to solve for $\underline{a}^+$ and $\underline{d}^-$. They are defined graphically in Fig. 3. The approaches indicated by a solid arrow are classified as the formulations of the first kind and those indicated by a dashed arrow are of the second kind. Although the eight ways of solution are theoretically equivalent, their numerical behaviors are somewhat different, especially when the magnetic wall is introduced at the upper half of the junction ($d = 0$, $\rho_n = 1$).

For general cases $d \neq 0$, all the formulations require a matrix inversion of size $(M \times M)$. For our limiting case of $d = 0$, special modifications must be made for some cases. Specifically, 1D and 2B need to invert a $(M + L) \times (M + L)$ matrix and 2C (Appendix A) needs to invert a smaller $(K \times K)$ matrix. Hence, 2C is most attractive to us because of its potential of numerical efficiency. In the next section, we will examine the various approaches in terms of the numerical stability and convergence.

## III. Numerical Results

To study the numerical behavior of the various formulations, we have chosen the structural parameters as: $a = 100$, $b = 26.1$ (in mils), $\epsilon_1 = 2.2$, $\epsilon_2 = 2.1$. The dominant mode (TEM) reflection and transmission coefficients at the junction are calculated by varying the matrix size for different $K/M$ ratios.

Since formulations 1D and 2B have an apparent disadvantage in numerical calculations, they are not considered here. After extensive studies, we have found that 1A, 1B, and 1C are numerically identical. Similarly, 2A and 2D are

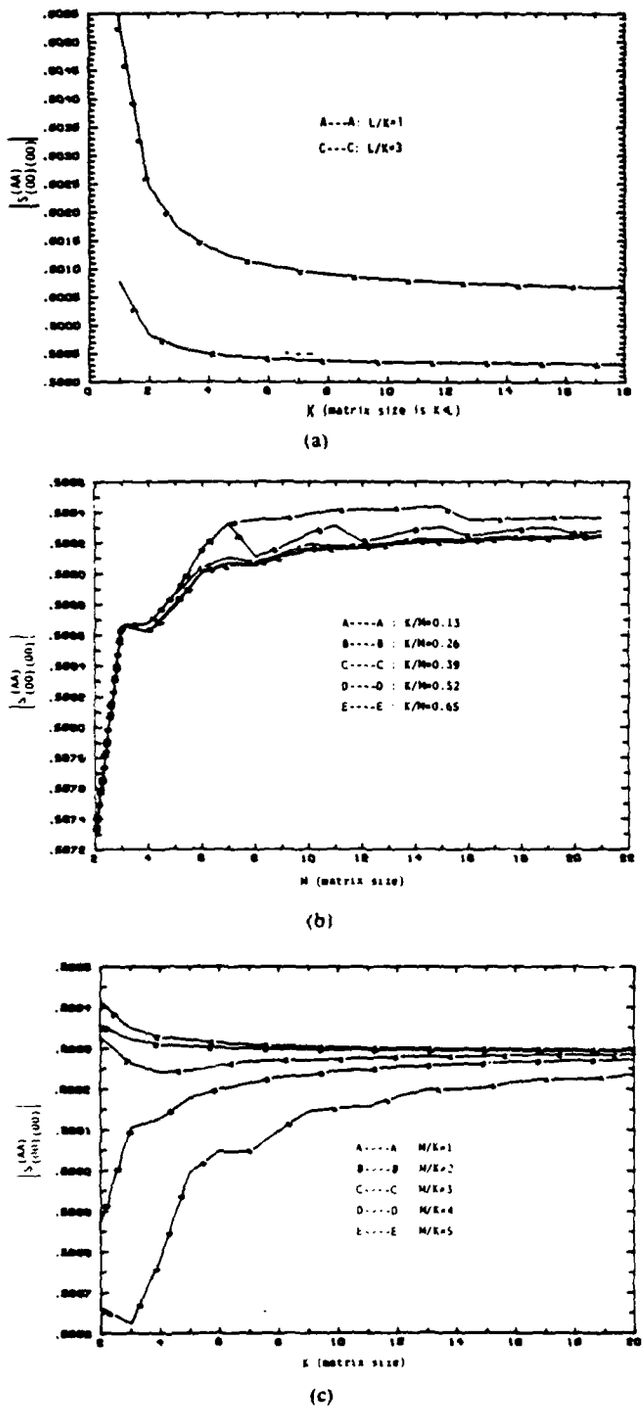


Fig. 4. Convergence study for various formulations: (a) formulation 1A; (b) formulation 2A; (c) formulation 2C.

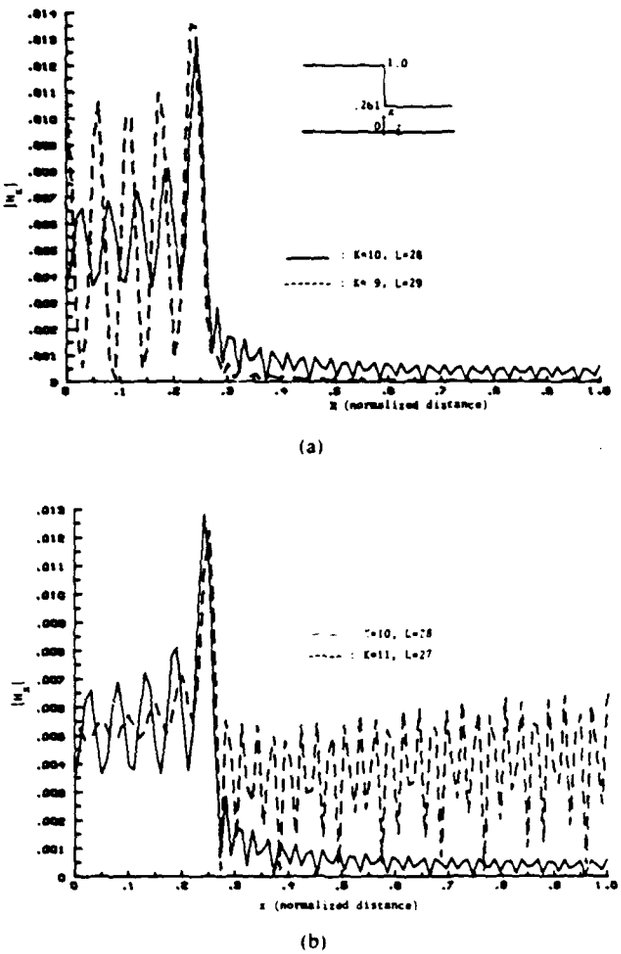


Fig. 5. Relative convergence problem of formulation 1A demonstrated by field plots.

numerically identical. Therefore, only three sets of data, corresponding to 1A, 2A, and 2C, are given.

In each formulation, the indices $L$, $K$, and $M$ are involved. The numerical results are affected by the ratios among these indices. This is called the relative convergence phenomenon, and it has been thoroughly discussed in the literature [4], [5]. It is well known that the best approximation to the true solution is obtained for $L/K = c/b = 73.6/26.1$ or $M/K = a/b = 100/26.1$ (refer to as the right ratio). It is observed that 2A and 2C suffer very little from the relative convergence problem (Fig. 4(b) and (c)). The problem is more serious in 1A, as can be seen in Fig. 4(a). With a ratio of one, the dominant mode reflection coefficient converges to an incorrect value (curve $A$ in Fig. 4(a)). Curve $C$ is calculated using a ratio of three, which is close to the right ratio.

The relative convergence effect can be more clearly observed from the plot of $H_x$ at the junction. The resultant field calculated by 1A is shown in Fig. 5. In Fig. 5(a), we plot the fields calculated using a ratio of $L/K = 28/10$ (very close to the right ratio) and a ratio of 29/9 (higher than the right ratio). In Fig. 5(b), we compare the field calculated using a ratio of 27/11 (lower than the right ratio) and a ratio of 28/10. It is interesting to note that, with a higher ratio, the calculated field behaves better on the magnetic wall discontinuity than on the aperture, while the opposite is true for field calculated using a lower ratio. This might seem reasonable because, for a higher ratio, we use more modes on the magnetic wall than on the aperture and vice versa for a lower ratio. Fig. 6 shows the resultant fields calculated by 2C. Different ratios have no noticeable effect. The fields calculated by 2A behave similar to those calculated by 2C.

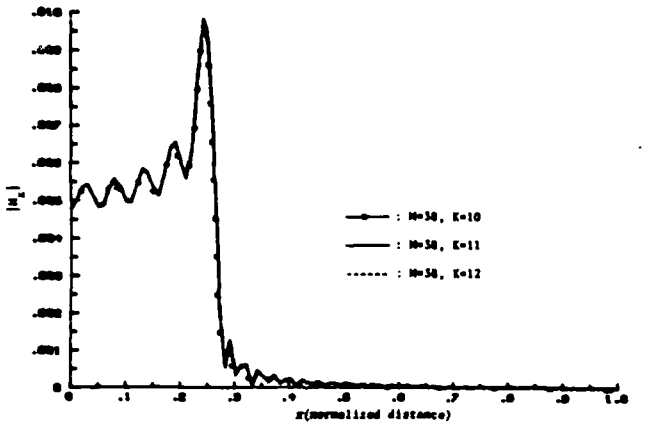


Fig. 6. Plot of fields calculated using formulation 2C with different $M/K$ ratios.

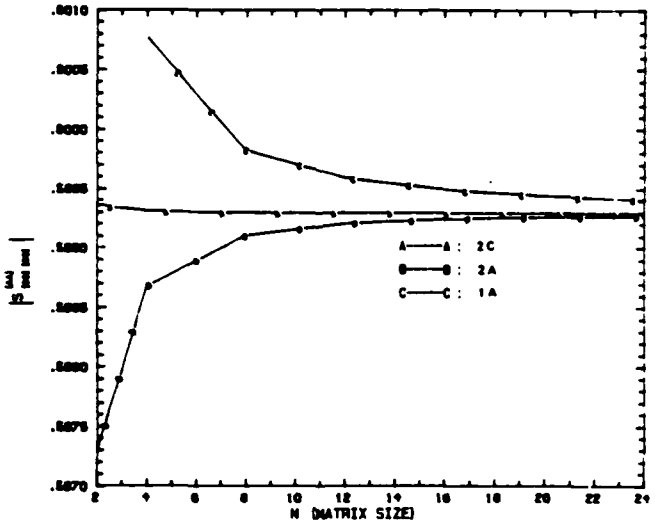


Fig. 7. Comparison of numerical efficiency.

A comparative study on the numerical efficiency for different approaches has also been done. In this case, $M/K = 4$, which is close to $a/b$, is chosen. The results of the dominant mode reflection coefficient $S[00][00]$ are evaluated as a function of the matrix size required and shown in Fig. 7. In addition, a comparison of how well the fields of the two sides match at the junction is done between formulations 2A and 2C. In both calculations, $M$ is set to 40, $K$ to 10. The result is shown in Fig. 8. The fields calculated by 2C match as well as, if not better than, those calculated by 2A. Keep in mind that we have to invert a matrix of size 40 in 2A, compared to a matrix of size 10 in 2C. It is now obvious that 2C has definite advantages over other approaches. This formulation is to be used for further studies.

Let us refer back to (2) at this point. In many attempts, $E_y$ in the region $b < x < a$ is not used as $H_x = 0$ there. This is identical to 2C and, hence, is our preferred choice.

To check the validity of our calculations, we have calculated the frequency response of a microstrip step discontinuity using the same parameters given by Kompa [2]. The results of the dominant mode reflection and transmission coefficients $S[00][00]$ and $S[00][00]$ are shown in Fig. 9. They are in good agreement with Kompa's results. The small discrepancy is due to the different formulas used for obtaining the effective width and effective dielectric constant of the waveguide model. Furthermore, we have checked the results with those independently obtained by the modified residue calculus technique [6]. The results of $S[00][00]$ are shown in Table I and Fig. 10 for comparison. The calculations are performed using Kompa's parameters.

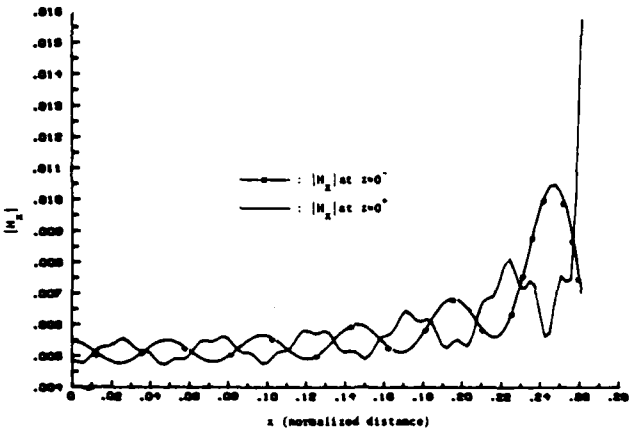


(a)

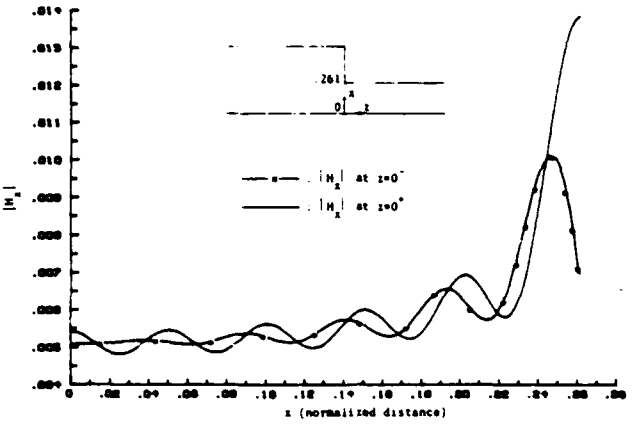


(b)

Fig. 8. Comparison of field plot between formulation 2A and 2C. (a) 2A, (b) 2C.

## IV. Conclusion

The mode-matching method has been applied to analyze the microstrip step-discontinuity problem based on the waveguide model. A comparison has been made among the various mode-matching solutions based on the matrix size and relative and absolute convergence. Although they are theoretically identical, one of them proves to be most suitable for numerical calculations. The results by this method are in good agreement with other published data and with those independently obtained by the modified residue calculus technique.

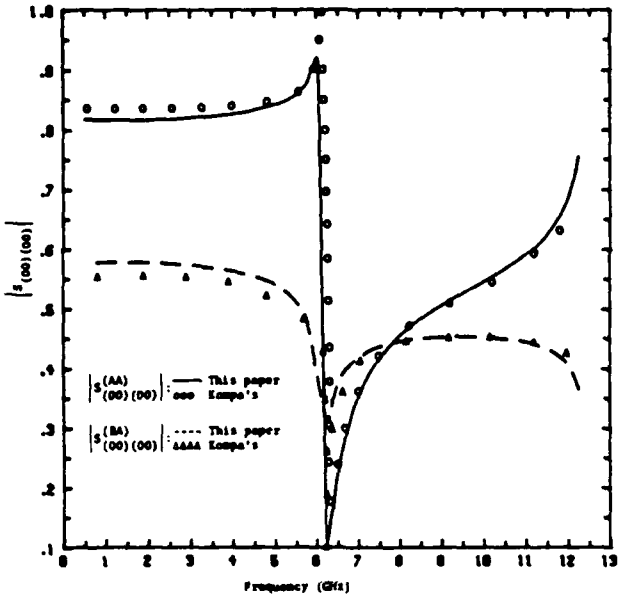


Fig. 9. Comparison with Kompa's results.

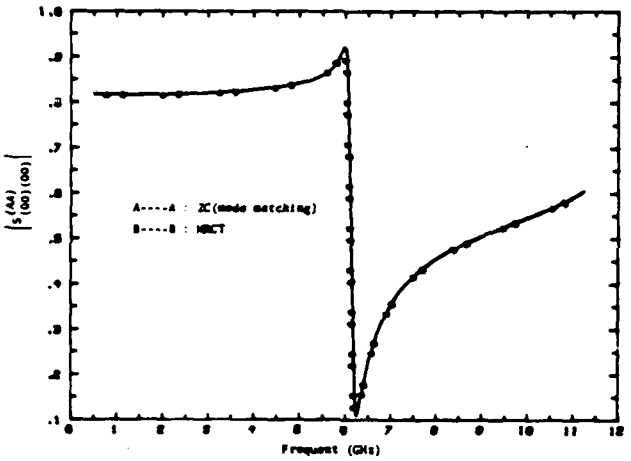


Fig. 10. Comparison with results of modified residue calculus technique.

TABLE I
COMPARISON OF THE RESULTS BY MODE-MATCHING METHOD AND BY MRCT*

| | Mode Matching | MRCT |
|---|---|---|
| $S_{(00)(00)}^{(AA)}$ | $0.1837 - j0.02291$ | $0.1837 - j0.02297$ |
| $S_{(00)(00)}^{(BA)}$ | $-0.7856 + j0.2227$ | $-0.7855 + j0.2233$ |

*Calculations are performed using Kompa's parameters at 2

## REFERENCES


[1] I. Wolff, G. Kompa, and R. Mehran, "Calculation method for microstrip discontinuities and T-junctions," *Electron. Lett.*, vol. 8, pp. 177–179, Apr. 1972.

[2] G. Kompa, "S-matrix computation of microstrip discontinuities with a planar waveguide model," *Arch. Elec. Ubertragung.*, vol. 30, pp. 58–64, 1975.

[3] W. Menzel and I. Wolff, "A method for calculating the frequency-dependent properties of microstrip discontinuities," *IEEE Trans. Microwave Theory Tech.*, vol. MTT-25, pp. 107–112, Feb. 1977.

[4] S. W. Lee, W. R. Jones, and J. J. Campbell, "Convergence of numerical solutions of iris-type discontinuity problems," *IEEE Trans. Microwave Theory Tech.*, vol. MTT-19, pp. 528–536, June 1971.

[5] R. Mittra, T. Itoh, and T. S. Li, "Analytical and numerical studies of the relative convergence phenomenon arising in the solution of an integral equation by the moment method," *IEEE Trans. Microwave Theory Tech.*, vol. MTT-20, pp. 96–104, Feb. 1972.

[6] T. S. Chu and T. Itoh, "Analysis of microstrip step discontinuity by the modified residue calculus technique," submitted to *IEEE Trans. Microwave Theory Tech.*, (Special Issue on Numerical Technique).


**Tak Sum Chu** was born in Kowloon, Hong Kong, on October 4, 1960. He received the B.S. degree in electrical engineering from the University of Texas at Austin in 1982. Currently, he is working towards the M.S. degree at the University of Texas.

**Tatsuo Itoh** (S'69–M'69–SM'74–F'82) received the Ph.D. degree in electrical engineering from the University of Illinois, Urbana, in 1969.

From September 1966 to April 1976, he was with the Electrical Engineering Department, University of Illinois. From April 1976 to August 1977, he was a Senior Research Engineer in the Radio Physics Laboratory, SRI International, Menlo Park, CA. From August 1977 to June 1978, he was an Associate Professor at the University of Kentucky, Lexington. In July 1978, he joined the faculty at the University of Texas at Austin, where he is now a Professor of Electrical and Computer Engineering and Director of the Electrical Engineering Research Laboratory. During the summer 1979, he was a Guest Researcher at AEG-Telefunken, Ulm, West Germany. Since September 1983, he has held the Hayden Head Centennial Professorship of Engineering at the University of Texas. Since September 1984, he has been Associate Chairman for Research and Planning of Electrical and Computer Engineering Department.

Dr. Itoh is a member of the Institute of Electronics and Communication Engineers of Japan, Sigma Xi, and Commission B of USNC/URSI. He serves on the Administrative Committee of IEEE Microwave Theory and Techniques Society and is the Editor of IEEE TRANSACTIONS ON MICROWAVE THEORY AND TECHNIQUES. He is a Professional Engineer registered in the State of Texas.

**Yi-Chi Shih** (S'80–M'82) was born in Taiwan, the Republic of China, on February 8, 1955. He received the B.Sc. degree from the National Taiwan University, Taiwan, R.O.C., 1976, the M.Sc. degree from the University of Ottawa, Ontario, Canada, in 1980, and the Ph.D. degree from the University of Texas at Austin, in 1982, all in electrical engineering.

In September 1982, he joined the faculty at the Naval Postgraduate School, Monterey, CA, as an Adjunct Professor of Electrical Engineering. Since April 1984, he has been with the Hughes Aircraft Company, Microwave Product Division, Torrance, CA, as a member of the technical staff.

# APPENDIX 2

# Generalized Scattering Matrix Method for Analysis of Cascaded and Offset Microstrip Step Discontinuities

TAK SUM CHU AND TATSUO ITOH, FELLOW, IEEE

*Abstract*—Detailed algorithms are presented for characterizations of cascaded microstrip step discontinuities, symmetric stubs, and offset step. The analysis is based on the generalized scattering matrix techniques after the equivalent waveguide model is introduced for the microstrip line.

## I. Introduction

THE EQUIVALENT waveguide model has been advantageously used for characterizing a number of discontinuities appearing in microstrip circuits [1]–[3]. Although the radiation and surface-wave excitation are neglected, these characterizations provide useful and accurate information in many practical applications. Formulations for these discontinuity problems are typically done by the mode-matching technique. However, detailed formulation algorithms are not readily available.

Recently, the present authors carried out an assessment for a number of different formulations for a microstrip step discontinuity within the framework of the waveguide model. The most economical and yet most accurate formulation was suggested [4]. The step discontinuity has also been analyzed by the modified residue calculus technique (MRCT) [5].

The present paper extends the analysis of the step discontinuity to a cascaded step discontinuity and an offset step discontinuity. The symmetric stub can be treated as the cascaded step discontinuity. The offset discontinuity will be treated as the limiting case of a cascaded discontinuity. In each case, the individual step discontinuity is characterized by either the MRCT or the mode-matching method. The analysis results in a generalized scattering matrix for each step. The analysis of the cascaded step is undertaken by invoking the generalized scattering matrix technique in which the generalized scattering matrices of two step junctions are combined [6], [7]. The ultimate result is the generalized scattering matrix of the cascaded junction as a whole.

It should be noted that the waveguide model is presumed to be an acceptable model for the present analysis. The results are compared with the experimental data as well as those reported in the literature.

Manuscript received August 2, 1985; revised October 1, 1985. This work was supported in part by the U.S. Army Research Office, under Contract DAAG29-84-K-0076.

The authors are with the Electrical Engineering Research Laboratory, University of Texas, Austin, TX 78712.

IEEE Log Number 8406468.

## II. Formulation of the Problem

### A. Cascaded Step Discontinuity

The algorithm for the analysis will be best illustr means of the cascaded step discontinuity. Specific required for the offset discontinuity will be explaine The first step of the analysis is to replace the mi circuit under study with its equivalent waveguide m The top and bottom are electric walls and the sidew magnetic walls. The height $h$ in Fig. 1 remains unc The effective dielectric constant $\epsilon_1$ and the effectiv $\overline{W}_1$ of region I with the microstrip width $W_1$ can b from the dominant mode phase constant $\beta_1$ and th acteristic impedance $Z_{01}$ of the microstrip line

$$\epsilon_1 = (\beta_1/k_0)^2$$

$$Z_{01} = \left[120\pi/\sqrt{\epsilon_1}\right](h/\overline{W}_1).$$

$\beta_1$ and $Z_{01}$ must be calculated from the structural p ters by a standard full-wave analysis [9], [10] or a c formula [11]. Other regions may be modeled in a manner.

The next step is to characterize all the discont involved in the waveguide model of the microstrip under study. This characterization is done in terms generalized scattering matrix [6], [7]. This matrix is related to the scattering matrix used in the mic network theory, but differes in that the dominant as higher order modes are included. Therefore, the alized scattering matrix will be, in general, of infinit Consider, for instance, the $TE_{p0}$ excitation with unit tude from the left to junction 1 in Fig. 2. If the am of the $n$th mode of the reflected wave to the left is $(n, p)$ entry of the scattering matrix $S^{11}(n, p)$ Similarly, if the amplitude of the $m$th mode of th transmitted to the right in $B_m$, $S^{21}(m, p)$ is $B_m$ matrix elements can be derived similarly. Hence, the alized scattering matrix $S_1$ of the junction 1 can be in terms of four submatrices of infinite order

$$S_1 = \begin{bmatrix} S^{11} & S^{12} \\ S^{21} & S^{22} \end{bmatrix}.$$

The corresponding matrix of the junction 2 is

$$S_2 = \begin{bmatrix} S^{33} & S^{34} \\ S^{43} & S^{44} \end{bmatrix}.$$

0018-9480/86/0200-0280$01.00 

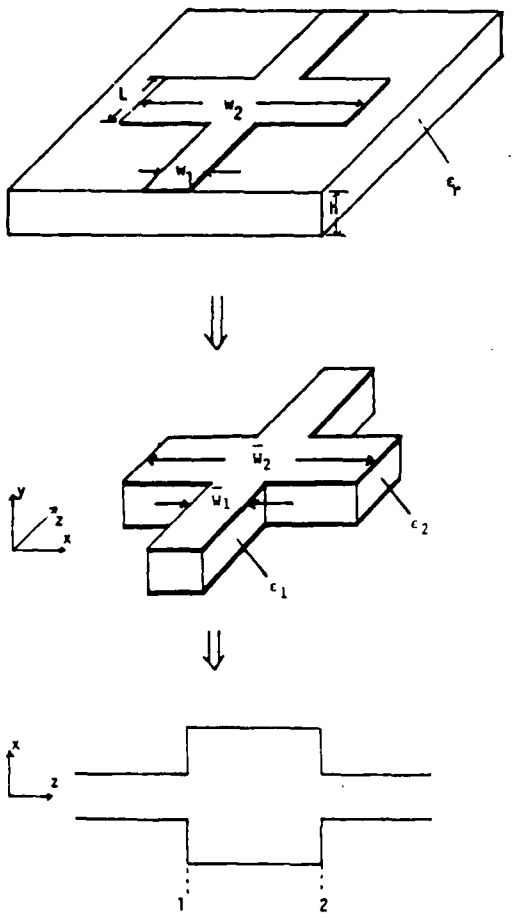


Fig. 1. Cascaded step discontinuities, equivalent waveguide model, and top view.

All of the elements of the generalized scattering matrix can be obtained by solving the electromagnetic problem of the junction scattering by means of a standard technique such as the mode-matching technique [4] or a modified residue calculus technique [5]. Since the details of these methods for an isolated step discontinuity are reported in [4] and [5], they are not repeated here. We presume all of these quantities are now available.

The remaining step is to combine these generalized scattering matrices of the cascaded junctions and to derive the composite matrix.

$$S = \begin{bmatrix} S^{AA} & S^{AC} \\ S^{CA} & S^{CC} \end{bmatrix}. \tag{5}$$

To this end, we introduce the transmission matrix $S^{(L)}$ of the waveguide between junctions 1 and 2. The wave travels a distance $L$ so that each mode is multiplied by $\exp(-\gamma L)$

$$S^{(L)} = \begin{bmatrix} e^{-\gamma_1 L} & & & 0 \\ & e^{-\gamma_2 L} & & \\ & & \ddots & \\ 0 & & & e^{-\gamma_n L} \end{bmatrix} \tag{6}$$

where $\gamma_n$ is the propagation constant of the $n$th mode of Region B. Hence $\gamma_1 = j\beta_2 L$, where $\beta_2$ is the dominant-mode phase constant of Region B. Our algebraic process to derive $S$ is detailed in the Appendix. The results are

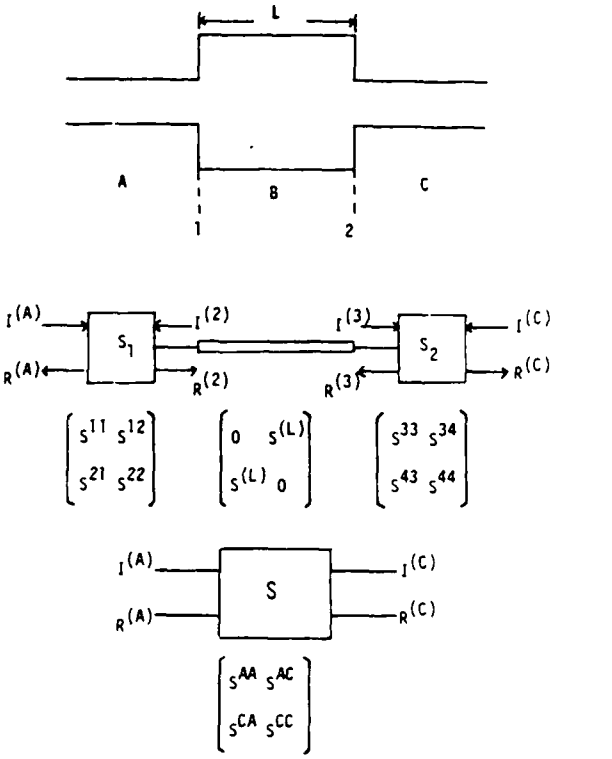


Fig. 2. Derivation of $S$ parameters for the cascaded step discontinuity structures.

$$S^{AA} = S^{11} + S^{12}S^{(L)}U_2S^{33}S^{(L)}S^{21} \tag{7a}$$

$$S^{AC} = S^{12}S^{(L)}U_2S^{34} \tag{7b}$$

$$S^{CA} = S^{43}S^{(L)}U_1S^{21} \tag{7c}$$

$$S^{CC} = S^{44} + S^{43}S^{(L)}U_1S^{22}S^{(L)}S^{34} \tag{7d}$$

where

$$U_1 = (I - S^{22}S^{(L)}S^{33}S^{(L)})^{-1} \tag{8a}$$

$$U_2 = (I - S^{33}S^{(L)}S^{22}S^{(L)})^{-1} \tag{8b}$$

and $I$ is the unit matrix. The above matrices are formally of infinite size. However, in practice, these matrices must be truncated to a finite size. It is found that excellent convergence is obtained when $3\times3$ or even $2\times2$ submatrices $S^{11}$, etc., are used.

It should be noted here that the use of generalized scattering matrices is increasingly more important as the distance between two junctions is smaller. Therefore, the present technique can be used for analysis of the symmetric stub from the knowledge of the generalized scattering matrix of a single step discontinuity.

### *B. Offset Step Discontinuity*

Next, the technique described above will be applied to an offset step discontinuity shown in Fig. 3. This offset discontinuity occurs in a microstrip circuit either intentionally or unintentionally. As we will see shortly, a small amount of offset $\Delta$ significantly affects the scattering characteristic of the discontinuity.

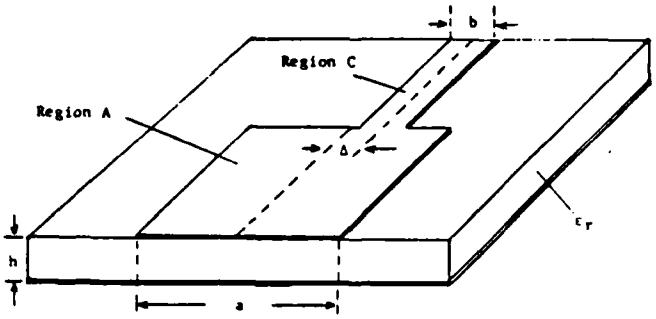


Fig. 3. Offset step discontinuity with eccentricity Δ.

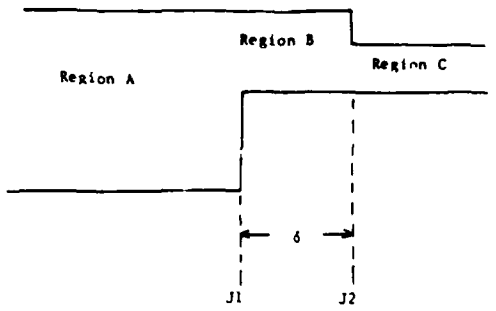


Fig. 5. Auxiliary structure of the offset step for the generalized scattering matrix technique.

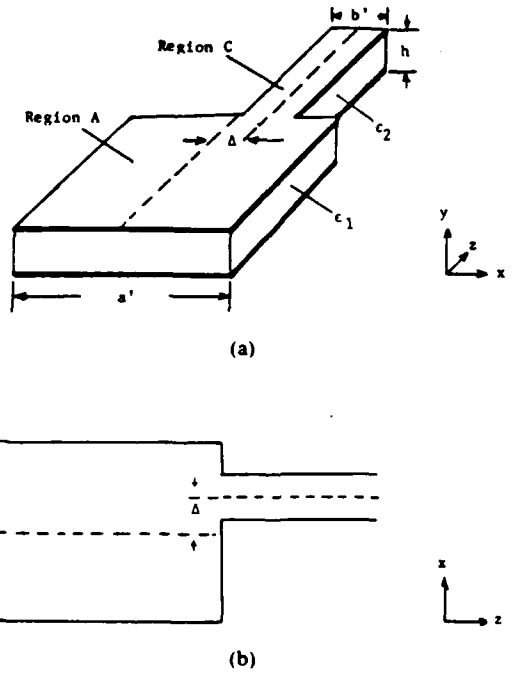


Fig. 4. Equivalent waveguide model of the offset step: (a) perspective view and (b) top view.

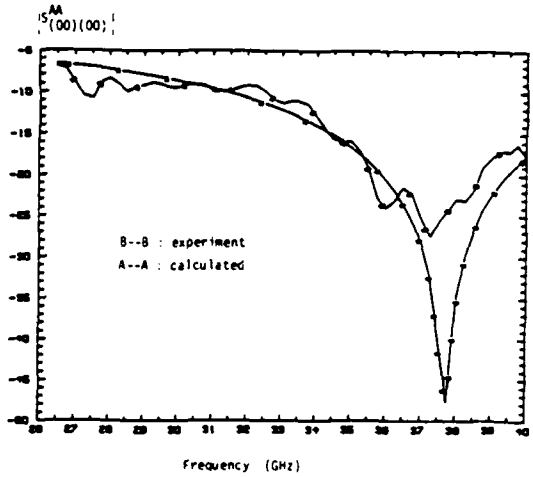


Fig. 6. Numerical data for the cascaded step.

## III. Results and Discussions

Fig. 6 shows typical results of the amplitude of the dominant mode (quasi-TEM) reflection coefficient from a cascaded step discontinuity. The results are found to agree very well with the experimental data taken at Hughes Torrance Research Center for the microstrip circuit on a Duroid substrate.

For efficient calculation, it is desirable to be able to truncate the matrices at as small a size as possible with accurate results. In the case of the cascaded discontinuity, $S^{(L)}$ contains a convergent factor since all of the higher order modes have real values of $\gamma_n$. In the case of an offset discontinuity, such exponentially decaying factors disappear because the length $\delta \to 0$, and hence $S^{(L)} = I$. To test the convergence of the solution, the dominant-mode transmission coefficient calculated using generalized scattering matrices of sizes $2\times2$, $3\times3$, and $5\times5$ are compared. Physical parameters are chosen to be the same as those studied by Kompa [12] so as to permit a comparison of results. Fig. 7 shows the results of this convergence study. It is seen that even the $2\times2$ matrix gives reasonably accurate results. To establish the validity of the results, they are compared with those calculated by Kompa [12]. This comparison is shown in Fig. 8(a) and (b). Finally, the dominant-mode transmission coefficient for various eccentricities are calculated. It is evident in Fig. 9 that the

Once again, the first step is to derive the equivalent waveguide model depicted in Fig. 4. Although a direct formulation of Fig. 4 is possible by way of the mode-matching technique, we will take an alternative approach in which the formulations and the generalized scattering matrices of the symmetric step discontinuities are advantageously used. To this end, an auxiliary structure in Fig. 5 is introduced. Notice that the original offset step discontinuity structure can be recovered by letting $\delta$ in Fig. 5 to zero after all the formulations are carried out. Also, the individual discontinuities $J1$ and $J2$ in Fig. 5 are one-half of the symmetric step discontinuities. Hence, all of the previous results for the symmetric step discontinuities excited by the even-mode can be directly used. In fact, in [4] and [5], only one-half of the structure has been used for analysis.

Once the scattering matrices of $J1$ and $J2$ are available, the scattering matrix of the composite discontinuity can be derived from (7) and (8) except that $S^{(L)} = I$ when $\delta \to 0$. This completes the formulation for the offset discontinuity.

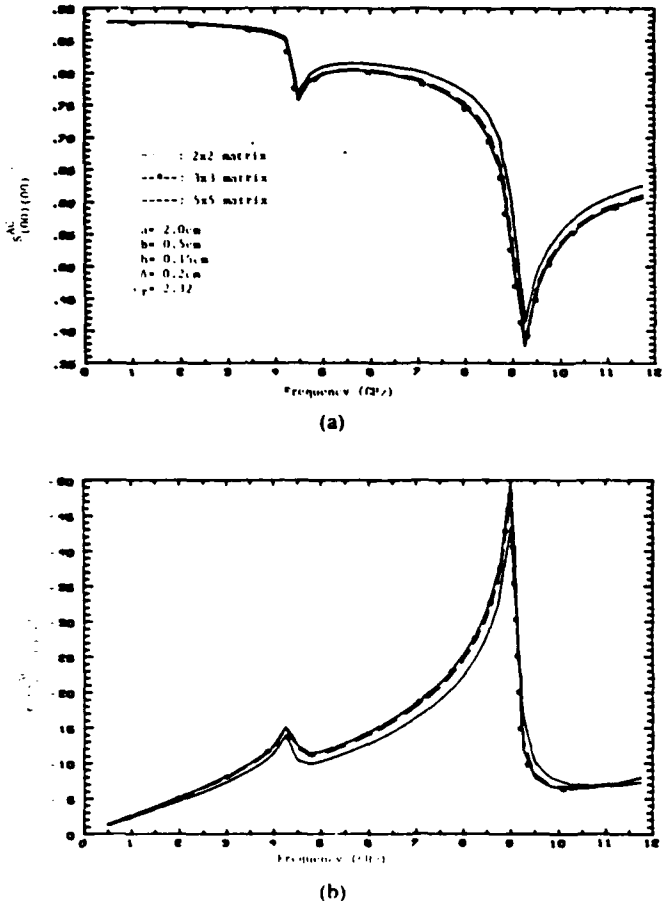


Fig. 7 Convergence study of the generalized scattering matrix technique for an offset step: (a) magnitude and (b) phase.

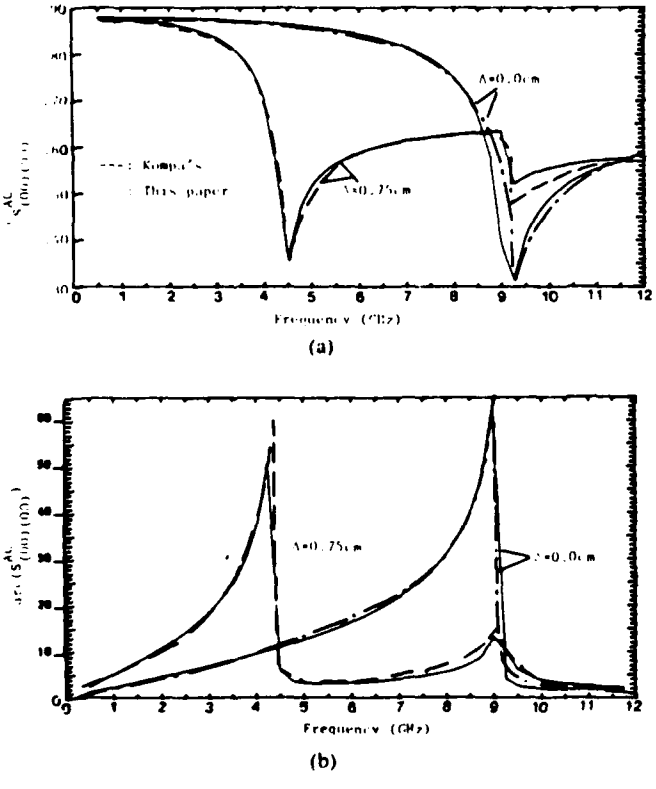


Fig. 8. Comparison with Kompa's results: (a) magnitude and (b) phase.

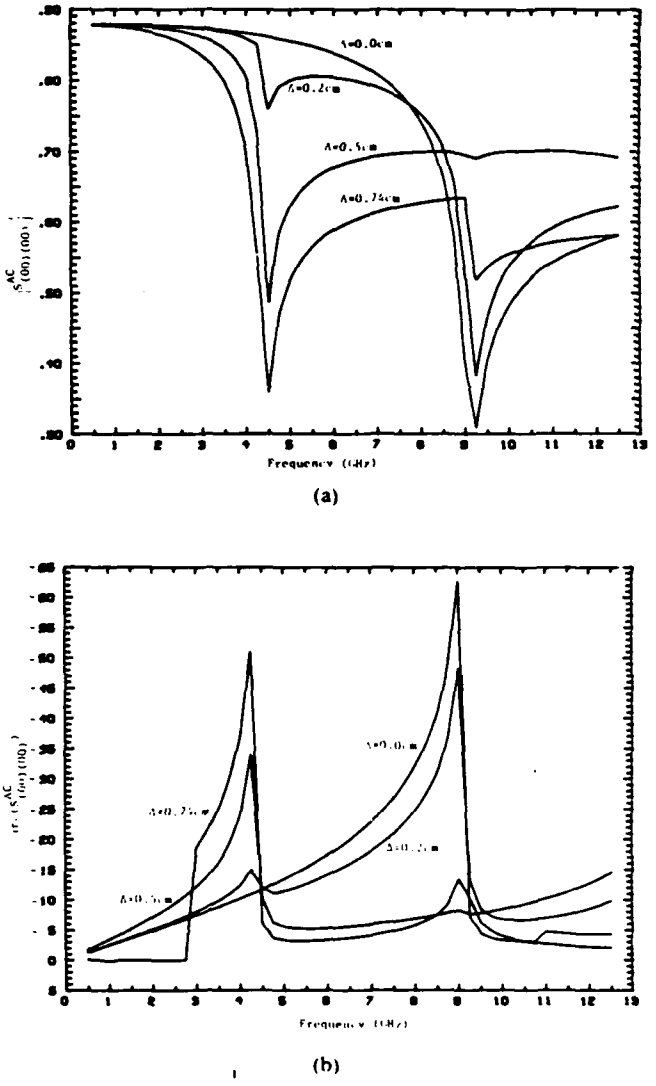


Fig. 9. Effect of eccentricity: (a) magnitude and (b) phase.

effect of the first odd-mode cutoff is exhibited as soon as the eccentricity is nonzero. Also, for $\Delta = 0.5$ cm, the effect of the second- (even-) mode cutoff is quite small due to the fact that the center of the smaller waveguide is located at the second-mode null and, hence, little coupling via this mode exists.

## IV. Conclusions

The generalized scattering matrix technique has been applied to the problems of a cascaded step discontinuity and an offset step discontinuity. The waveguide model has been presumed to be applicable for analysis. Individual discontinuities are characterized first and the results are used for the description of the composite discontinuity via the generalized scattering matrix technique. In spite of the two-step process, the overall effort in numerical processing is quite efficient. In actual numerical software, the programs for isolated discontinuities can be used as subroutines for the composite structures.

## APPENDIX
## DERIVATION OF SCATTERING MATRIX FOR THE CASCADED STEP DISCONTINUITIES

The following matrix equations can be derived from Fig. 2:

$$\begin{bmatrix} R^{(A)} \\ R^{(2)} \end{bmatrix} = \begin{bmatrix} S^{11} & S^{12} \\ S^{21} & S^{22} \end{bmatrix} \begin{bmatrix} I^{(A)} \\ I^{(2)} \end{bmatrix} \tag{A1}$$

$$\begin{bmatrix} I^{(2)} \\ I^{(3)} \end{bmatrix} = \begin{bmatrix} 0 & S^{(L)} \\ S^{(L)} & 0 \end{bmatrix} \begin{bmatrix} R^{(2)} \\ R^{(3)} \end{bmatrix} \tag{A2}$$

$$\begin{bmatrix} R^{(3)} \\ R^{(C)} \end{bmatrix} = \begin{bmatrix} S^{33} & S^{34} \\ S^{43} & S^{44} \end{bmatrix} \begin{bmatrix} I^{(3)} \\ I^{(C)} \end{bmatrix}. \tag{A3}$$

Next, (A2) is substituted into (A1) to get

$$R^{(A)} = S^{11}I^{(A)} + S^{12}S^{(L)}R^{(3)} \tag{A4}$$

$$R^{(2)} = S^{21}I^{(A)} + S^{22}S^{(L)}R^{(3)}. \tag{A5}$$

Next, (A2) is substituted into (A3) to get

$$R^{(3)} = S^{33}S^{(L)}R^{(2)} + S^{34}I^{(C)} \tag{A6}$$

$$R^{(C)} = S^{43}S^{(L)}R^{(2)} + S^{44}I^{(C)}. \tag{A7}$$

Equations (A5) and (A6) are used to isolate $R^{(2)}$ and $R^{(3)}$

$$R^{(2)} = U_1S^{21}I^{(A)} + U_1S^{22}S^{(L)}S^{34}I^{(C)} \tag{A8}$$

where

$$U_1 = (I - S^{22}S^{(L)}S^{33}S^{(L)})^{-1}$$

and

$$R^{(3)} = U_2S^{33}S^{(L)}S^{21}I^{(A)} + U_2S^{34}I^{(C)} \tag{A9}$$

where

$$U_2 = (I - S^{33}S^{(L)}S^{22}S^{(L)})^{-1}.$$

Finally, (A8) and (A9) are substituted into (A4) and (A7) to get

$$R^{(A)} = S^{11}I^{(A)} + S^{12}S^{(L)}U_2S^{33}S^{(L)}S^{21}I^{(A)} + S^{12}S^{(L)}U_2S^{34}I^{(C)}$$

$$R^{(C)} = S^{43}S^{(L)}U_1S^{21}I^{(A)} + S^{43}S^{(L)}U_1S^{22}S^{(L)}S^{34}I^{(C)} + S^{44}I^{(C)}.$$

$S^{AA}$, $S^{AC}$, $S^{CA}$, and $S^{CC}$ can be identified easily from the above equations.

## ACKNOWLEDGMENT

The authors thank Dr. Y. C. Shih of Hughes Torrance Research Center for providing experimental data and for technical discussions.

## REFERENCES

[1] I. Wolff, G. Kompa, and R. Mehran, "Calculation method for microstrip discontinuities and T-junctions," *Electron. Lett.*, vol. 8, pp. 177–179, Apr. 1972.

[2] G. Kompa, "S-matrix computation of microstrip discontinuities with a planar waveguide model," *Arch. Elek. Übertragung.*, vol. 30, pp. 58–64, Feb. 1976.

[3] W. Menzel and I. Wolff, "A method for calculating the frequency-dependent properties of microstrip discontinuities," *IEEE Trans. Microwave Theory Tech.*, vol. MTT-25, pp. 107–112, Feb. 1977.

[4] T. S. Chu, T. Itoh, and Y-C. Shih, "Comparative study of mode-matching formulations for microstrip discontinuity problems," *IEEE Trans. Microwave Theory Tech.*, vol. MTT-33, pp. 1018–1023, Oct. 1985.

[5] T. S. Chu and T. Itoh, "Analysis of microstrip step discontinuity by the modified residue calculus technique," *IEEE Trans. Microwave Theory Tech.*, vol. MTT-33, pp. 1024–1028, Oct. 1985.

[6] J. Pace and R. Mittra, "Generalized scattering matrix analysis of waveguide discontinuity problems," in *Quasi-Optics XIV*. New York: Polytechnic Institute of Brooklyn Press, 1964, pp. 172–194.

[7] Y.-C. Shih, T. Itoh, and L. Q. Bui, "Computer-aided design of millimeter-wave E-plane filters," *IEEE Trans. Microwave Theory Tech.*, vol. MTT-31, pp. 135–142, Feb. 1983.

[8] I. Wolff and N. Knoppik, "Rectangular and circular microstrip disk capacitors and resonators," *IEEE Trans. Microwave Theory Tech.*, vol. MTT-22, pp. 857–864, Oct. 1974.

[9] T. Itoh, "Spectral domain immittance approach for dispersion characteristics of generalized printed transmission lines," *IEEE Trans. Microwave Theory Tech.*, vol. MTT-28, pp. 733–736, July 1980.

[10] R. Jansen and M. Kirschning, "Arguments and an accurate model for the power-current formulation of microstrip characteristic impedance," *Arch. Elek. Übertragung.*, vol. 37, pp. 108–112, Mar. 1983.

[11] E. Hammerstad and O. Jensen, "Accurate models for microstrip computer-aided design," in *IEEE MTT-S Int. Symp. Dig.* (Washington, DC), 1980, pp. 407–409.

[12] G. Kompa, "Frequency-dependent behavior of microstrip offset junction," *Electron. Lett.*, vol. 11, no. 22, pp. 172–194, Oct. 1975.

**Tak Sum Chu** was born in Kowloon, Hong Kong, on October 4, 1960. He received the B.S. degree in electrical engineering from the University of Texas at Austin in 1982. Currently, he is working towards the M.S. degree at the University of Texas.

**Tatsuo Itoh** (S'69–M'69–SM'74–F'82) received the Ph.D. degree in electrical engineering from the University of Illinois, Urbana, in 1969.

From September 1966 to April 1976, he was with the Electrical Engineering Department, University of Illinois. From April 1976 to August 1077, he was a Senior Research Engineer in the Radio Physics Laboratory, SRI International, Menlo Park, CA. From August 1977 to June 1978, he was an Associate Professor at the University of Kentucky, Lexington. In July 1978, he joined the faculty of the University of Texas at Austin, where he is now a Professor of Electrical Engineering and Director of the Microwave Laboratory. During the summer of 1979, he was a Guest Researcher at AEG-Telefunken, Ulm, West Germany. Since 1983, he has held the Hayden Head Professorship in Engineering.

Dr. Itoh is a member of the Institute of Electronics and Communication Engineers of Japan, Sigma Xi, and Commissions B and C of USNC/URSI. He is a Professional Engineer registered in the State of Texas.

# APPENDIX 3

# Microstrip-Fed Planar Frequency-Multiplying Space Combiner

S. NAM, TOMOKI UWANO, MEMBER, IEEE, AND TASUO ITOH, FELLOW, IEEE

*Abstract*—A frequency-multiplying power combining array has been made of slots in the ground plane on a substrate with a microstrip feedline on the back side. The second harmonic generated by a diode in each slot is combined in free space. A design procedure and experimental results are presented.

## I. Introduction

GENERATION OF a coherent millimeter-wave signal with a reasonable strength becomes more difficult as the frequency of operation is increased. One of the methods to alleviate this problem is the use of a power combining technique [1]. However, it is increasingly difficult to combine the power outputs from more than a few devices. In many power combining schemes, very involved design procedures, complicated fabrication, and tricky postfabrication tuning are required. An alternative approach is the use of frequency multiplication [2]. In this approach, the output power level is substantially lower than the input signal level. In addition, the power level that can be handled by a diode-type frequency multiplier is quite limited. To alleviate many of the deficiencies described above, a quasi-optical frequency-multiplying space power combiner has been proposed and tested [3]. The proposed structure contains in a single component (1) a slot antenna array, (2) frequency multipliers, and (3) a power combiner. The structure has a simple configuration and requires no bias and no postproduction tuning.

In this paper, a new printed circuit configuration of the frequency-multiplying space power combiner is presented. In contrast to the work in [3], no waveguide is used for feeding. In the new structure, the array of slots on the substrate is fed by a microstrip line or a coplanar waveguide fabricated on the back side of the substrate. The new structure has other desirable features, such as (1) a planar structure suitable for monolithic integration, (2) large coupling, (3) controllable coupling, and (4) flexibility in the arrangement of slots on a planar circuit.

Fig. 1 shows a typical configuration of the planar multiplier/combiner. On the front side of the substrate, there is an array of slots and in each of these a diode is placed for frequency multiplication. A microstrip line feed on the back side is used in this example. The incident signal at the frequency $f_0$ is successively fed to these slots, which are typically a quarter wavelength long. The diode in each slot generates a second harmonic of $2f_0$. Then the slot behaves as a half wave slot dipole and an efficient radiation of a $2f_0$ signal takes place. The radiated powers from all the slots are combined in free space. This paper reports an experimental design of the structures scaled for a low-frequency operation at the $X$-band. This scaling allows us to use more precise characterizations than those attainable at millimeter-wave frequencies, so that useful design data can be collected more efficiently.

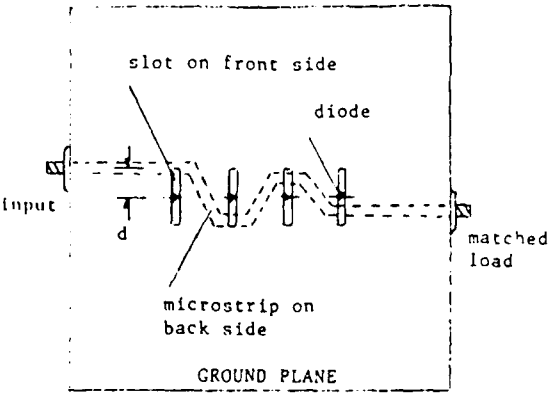


Fig. 1. Structure of multiplying slot array fed by microstrip.

## II. Design Procedure

In order to design the proposed structure, it is necessary to know the characteristics of the microstrip-to-slot transition, the phase relationship between slots, and the conversion gain of each slot. Let us first study these characteristics in detail.

### A. Magnitude Characteristics of Microstrip-to-Slot Transition

The transition characteristics have been studied based on the approximate equivalent circuit shown in Fig. 2 [4]. The magnitude characteristics of the coupling from the microstrip to the slot, the insertion loss of the slot, and the return loss of the slot with a 50-Ω load located at the

Manuscript received March 23, 1987; revised August 17, 1987. This work was supported in part by the U.S. Army Research Office under Contract DAAG-84-K-0076.

S. Nam and T. Itoh are with the Department of Electrical and Computer Engineering, University of Texas, Austin, TX 78712.

T. Uwano was with the University of Texas at Austin, on leave from the Matsushita Electric Ind. Co., Ltd., Osaka 571, Japan.

IEEE Log Number 8717394

0018-9480/87/1200-1271$01.00 

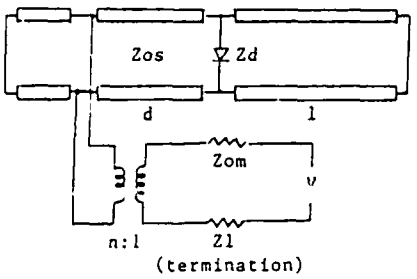


Fig. 2. Equivalent circuit for one slot ($l = \lambda_0/8$).

center of the slot are given as follows:

$$\text{Coupling} = 20\log\left|2nZ(\cos\beta d + \tan\beta d \sin\beta d)\right.$$
$$\left./((Z_{0m} + Z_L + Z)(1 + jZ_{0s}\tan\beta d/Z_3))\right| \quad (1)$$

$$\text{Insertion loss} = 20\log|2Z_L(Z_{0m} + Z_L + Z)| \quad (2)$$

$$\text{Return loss} = 20\log|(Z_{0m} - Z - Z_L)/(Z_{0m} + Z + Z_L)| \quad (3)$$

where

$Z$ slot impedance seen from the microstrip,
$Z_{0m}$ characteristic impedance of the microstrip,
$Z_{0s}$ characteristic impedance of the slot line,
$Z_L$ termination impedance (50 Ω),
$Z_3$ slot impedance seen from the center of the slot.

According to the calculated results, the smaller the distance from the center of the slot to the feeding position, the larger the coupling becomes. In order to examine the possibility of controlling the power coupled from the microstrip to the slot, we measured the transition characteristics. Measurement of microstrip-to-slot transition has been carried out with the conventional coaxial-to-slotline transition [5] as a probe for picking up the signal over the slot in place of the diode. From the measurement results, it is found that the control of the power coupled from the microstrip to the slot is possible by controlling the distance from the center of the slot to the feeding position. Also, it is seen that the equivalent circuit for the transition gives a prediction that agrees well with the measured data, if $n = 1$ is chosen, as long as the feeding position is not too close to the end of the slot. The results are shown in Fig. 3. The dotted lines show the calculated results under the assumption of $n = 1$ in Fig. 2.

### B. Phase Relationship between Slots

The phase relationship between slots is determined by (1) the electrical length of the microstrip feed line between slots, (2) the phase characteristics of the transition, and (3) the square-law characteristics of the diode. Among these factors, the main contribution is the electrical length of the microstrip feedline between the slots. This quantity can be controlled by the physical length of the microstrip line between the slots.

The phase characteristics of the transition can be evaluated from the phase change of the voltage from the

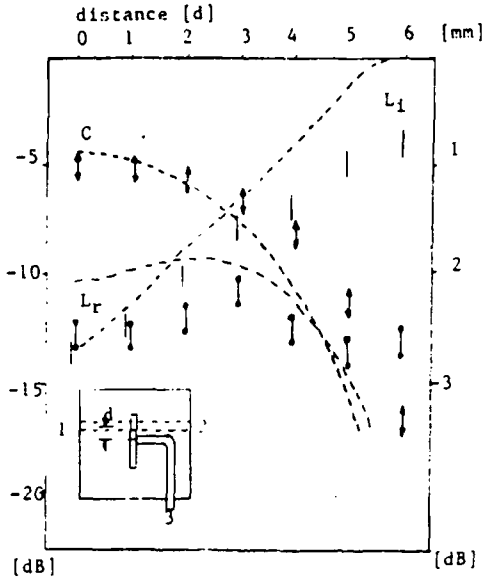


(a)

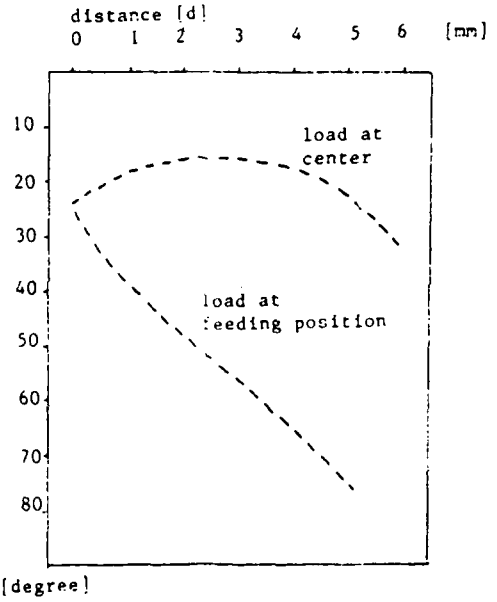


(b)

Fig. 3. Transition characteristics from microstrip to slot. (a) Coupling ($C$), insertion loss ($L_i$), and return loss ($L_r$). (b) Phase change of transition with load position.

transition point of the microstrip to the 50-Ω load on the slot by the following equation:

$$\text{Phase change} = \arg\left[2nZ_L\cos\beta d + \tan\beta d \sin\beta d)\right.$$
$$\left./((Z_{0m} + Z_L + Z)(1 + jZ_{0s}\tan\beta d/Z_3))\right]. \quad (4)$$

The results are plotted in Fig. 3(b) as a function of the position of the load. From these results, we find that the difference of the phase change to the feeding position can be neglected if the load is located at the center of the slot.

A diode located across the slot can be thought to pick up the voltage of the input frequency signal. The voltage

on the slot forms a standing wave pattern given by

$$V(x) = \sin\beta(d + l_h - x)/\sin\beta(d + l_h). \quad (5)$$

Since this voltage has a maximum value at the feeding position, it is better to locate the diode at the feeding position for a better matching and a stronger coupling. As shown in Fig. 3(b), the phase change of voltage versus feeding position of each transition cannot be neglected in this case. Therefore, it is required that the difference of the phase change at each transition be considered for determination of the length of the microstrip line between the slots.

In the case of a two-element slot array, the length of the microstrip feed line between the slots is $\lambda_g/2$, where $\lambda_g$ is the guide wavelength at the input frequency. However, the diodes should be placed with the same polarity at each slot for the broadside operation. This can be explained by the square-law behavior of the diode [3].

### C. Conversion Gain of Each Slot

The conversion gain of a multiplier is defined as the ratio of the output power to the input power. In the present case, the input power is the amount of power coupled to a single slot from the microstrip at the fundamental frequency. The output power is the amount of the power at the second harmonic frequency, which is radiated by this slot into free space. Thus, we have to evaluate the amounts of input power and radiated power to find the conversion gain. The impedance of the mixer diode used in this paper is a function of the drive power. However, if the diode is driven sufficiently (more than 10 dBm), the impedance is known to be about 50 Ω. Thus, the power coupled into the diode at the fundamental frequency can be estimated by using $C$ in Fig. 3(a). The direct measurement of the amount of the radiated output power is very difficult. Hence, we use an indirect method based on the fact that the power received at a fixed receiving antenna is proportional to the output power of a transmitting antenna. This relation is given by [6]

$$P_r = P_t + G_t + K \quad (6)$$

where

- $P_r$ receive power (dBm),
- $P_t$ transmit power (dBm),
- $G_t$ transmit antenna gain (dB),
- $K$ constant determined by the gain of receiving antenna, distance between the transmitting antenna and the receiving antenna, and the test frequency.

For the DUT (device under test), the transmit power can be expressed by

$$P_{t,d} = P_{i,d} + C_d + G_c \quad (7)$$

- $P_{t,d}$ transmit power (dBm) from DUT,
- $P_{i,d}$ incident power (dBm) to the microstrip feed line in DUT,
- $C_d$ power coupling factor (dB) to diode in DUT,
- $G_c$ conversion gain (dB) of DUT.

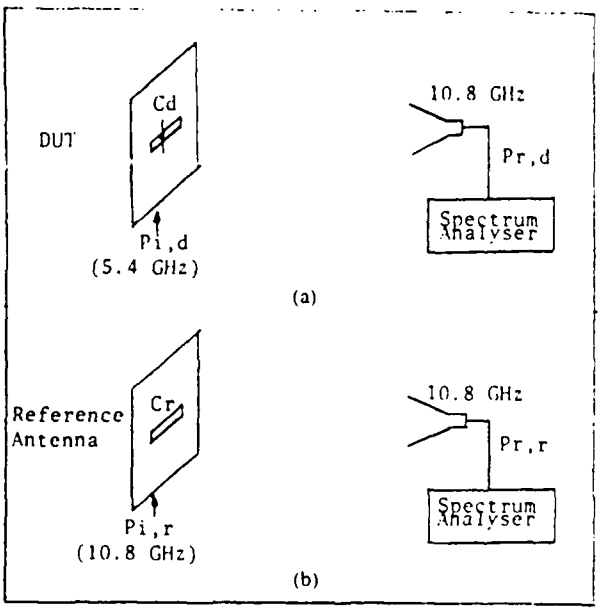


Fig. 4. Test setup for measuring the multiplication conversion gain. (a) DUT setup. (b) Reference setup.

Using (7), the power relation applied to the DUT setup shown in Fig. 4(a) is given by

$$P_{r,d} = (P_{i,d} + C_d + G_c) + G_{t,d} + K \quad (8)$$

where

- $P_{r,d}$ receive power (dBm) in DUT setup,
- $G_{t,d}$ antenna gain (dB) of DUT.

For the reference antenna, the transmit power can be expressed by

$$P_{t,r} = P_{i,r} + C_r \quad (9)$$

where

- $P_{t,r}$ transmit power (dBm) of reference antenna,
- $P_{i,r}$ incident power (dBm) to the microstrip feed line in reference antenna,
- $C_r$ power coupling factor (dB) to reference antenna.

Using (9), the power relation applied to reference setup shown in Fig. 4(b) is given by

$$P_{r,r} = (P_{i,r} + C_r) + G_{t,r} + K \quad (10)$$

where

- $P_{r,r}$ receive power (dBm) in reference setup,
- $G_{t,r}$ gain (dB) of reference antenna.

Using (8) and (10), the conversion gain can be calculated from

$$G_c = P_{r,d} - P_{r,r} - P_{i,d} + P_{i,r} - C_d + C_r - G_{t,d} + G_{t,r}. \quad (11)$$

### D. Design Procedure

Let us consider the design procedure of the multiplying slot array. Coupling is defined by

$$\text{Coupling} = P_{\text{diode}} - P_{\text{input}} \quad [\text{dB}]. \quad (12)$$

For simplicity, we locate all the diodes at the center of each slot and design an equally excited, broadside multiplying slot array by applying (12) to the measured results in Fig. 3. First, from the power requirement of the diode in the first slot, we calculate the necessary coupling by (12); then we evaluate the location of the microstrip-to-slot transition from $C$ in Fig. 3(a). We can then find out the amount of power left over on the microstrip line from $L_1$ in Fig. 3(a). Next, we find the location of the transition of the second slot so that the power provided to the second diode is equal to that for the first diode. Then, we determine the length of the microstrip to the second slot to obtain an appropriate phase shift between slots. This process is repeated until all the slots are taken care of. Notice from Fig. 1 that the location of the transition moves inward as the feed signal progresses along the microstrip line. The decreasing power available from the feed line is compensated for by an increasing degree of coupling so that all the diodes are given an equal excitation power. It is possible to design various multiplying slot array antennas with a suitable arrangement of multiplying slots in the ground plane with the proper excitation powers and phase differences [6]. These design quantities can be obtained by controlling the locations of the transitions and the lengths of the microstrip between the slots.

## III. Experimental Results

For frequency multiplication, nonlinear reactive elements such as varactor diodes are desirable for achieving good performance. However, only the Schottky-barrier diodes designed for $X$-band mixers have been available to the authors. The conversion gain, $G_c$, measured by the method described above for the structure with the ND5051(NEC) diode has been $-6.2$ dB. In this experiment, the power coupling factor to the reference antenna, $C_r$, can be estimated by

$$C_r = 10 \log \left[ (P_{in} - P_{ref} - P_{tra}) / P_{in} \right] \qquad (13)$$

where

- $P_{in}$ incident power (mW) to microstrip feed line in reference antenna,
- $P_{ref}$ reflected power (mW) at input port in reference antenna,
- $P_{tra}$ transferred power (mW) to the matching load in reference antenna.

An estimated power coupling factor of $-7$ dB results. Note that the only difference in antenna structure between the DUT and the reference antenna is that there is a diode in the DUT while there is no diode in the reference antenna. This fact causes a difference in the gain of the two antennas. The difference of the two antenna gains can be estimated by measuring the reduction of the receiving power in the reference setup shown in Fig. 4(b) when a diode is located at the center of the slot of the reference antenna. About 10 dB reduction in the antenna gain due to the loading effect of the diode is measured.

For the other higher order harmonics generated by the diode, the slot can also be thought of as a slot dipole antenna. However it is observed that the receiving power of the third harmonic signal is lower than that of the second harmonic signal by more than 10 dB.

In order to design the multiplying slot array antenna, it is necessary to know the characteristics of the element radiation pattern of the single multiplying slot antenna. First, the effect of the ground plane size is evaluated. Fig. 5(a) shows the radiation patterns of a single slot antenna with a ground plane of different sizes. It is found that the length of one side of the ground plane should be larger than seven wavelengths at the radiating frequency (about 20 cm at 10.8 GHz). Otherwise, the element radiation pattern of the slot antenna has several peaks and valleys. This effect of the finite ground plane on the radiation by a slot can be explained theoretically by the uniform theory of diffraction [6]. Next, the effect of the location of the transition is tested. Fig. 5(b) shows the radiation patterns of a single multiplying slot antenna with the transition at different locations. We notice that the position of the feeding point has a negligible influence on the radiation pattern. This is due to the fact that for the second harmonic signal, the diode located at the center of the slot can be considered a source. Even though its output power is dependent on the feeding position, its position on the slot is not changed with the feeding position. Therefore, the radiation power of the multiplying slot antenna is changed with the feeding position but the radiation pattern for the front space of the slot seems to be insensitive to the position of the narrow microstrip feed line on the back side.

For the loading effect of the diode on the radiation pattern, the radiation patterns of the single slot antenna with the diode and without the diode are measured. By comparing Fig. 5(b) with Fig. 5(a), we notice that the diode located at the center of the slot reduces the number of undulations in the radiation pattern. However, the overall radiation pattern is not changed.

Based on the experimental transition characteristics and the elementary radiation pattern of the single slot, we designed and tested several uniformly excited broadside multiplying slot arrays. Figs. 5(c) and (d) show the radiation patterns of a two-element $H$-plane slot array antenna for different spacings between the slots. It is observed that the radiation pattern of an $H$-plane array with more closely spaced elements shifts more from the broadside direction. This is due to the increased internal mutual interference between the slots. The spacing between $H$-plane slots should be more than one wavelength at the second harmonic frequency to avoid interference. However, this requirement produces grating lobes in pairs for a broadside antenna. For the design of an array with closer spacing, it is necessary to measure the element radiation pattern including the effect of internal interference. Figs. 5(e) and (f) show the radiation patterns of a two-element $E$-plane slot array antenna with different degrees of coupling. It is observed that the radiation pattern of an array

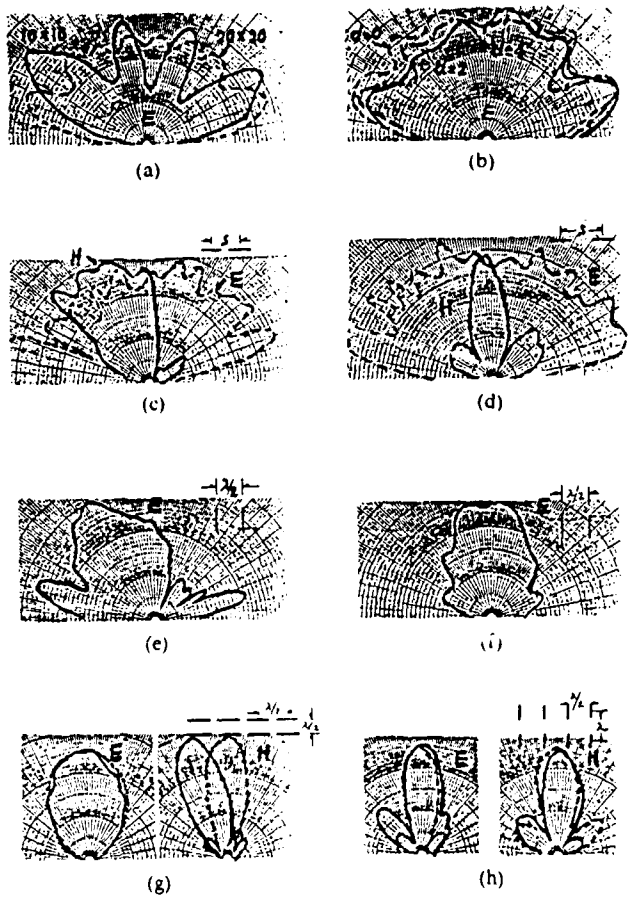


Fig. 5. Measured radiation patterns of various multiplying slot antennas. (The magnitude is plotted in linear scale.) (a) Radiation pattern of a single multiplying slot antenna for different ground plane sizes (without diode). (b) Radiation pattern of a single multiplying slot antenna for different feeding positions (with diode, $20 \times 20$). (c) Radiation pattern of a two-element $H$-plane slot array antenna (spacing = $\lambda/2$). (d) Radiation pattern of a two-element $H$-plane slot array antenna (spacing = $\lambda$). (e) Radiation pattern of a two-element $E$-plane slot array antenna for large coupling ($-5$ dB). (f) Radiation pattern of a two-element $E$-plane slot array antenna for small coupling ($-10$ dB). (g) Radiation pattern of a $2 \times 4$ $H$-plane slot array antenna. (h) Radiation pattern of a $2 \times 4$ $E$-plane slot array antenna. (The dotted lines indicate calculated radiation pattern.)

with more strongly excited slot elements shifts more from the broadside direction. This is because the reflected power at the transition is increased as the coupling increases and because the neglected phase shift at the microstrip-to-slot transition is increased as the difference of the feeding positions at the two slots increases.

Figs. 5(g) and (h) show the radiation patterns of the $2 \times 4$ $H$-plane and the $2 \times 4$ $E$-plane slot arrays with the calculated radiation patterns, respectively. The measured radiation patterns agree well with the theoretical results except for the $H$-plane radiation pattern of the $2 \times 4$ $H$-plane slot array. The reason for this is explained above. These arrays are excited with the incident power of 26 dBm at 5.4 GHz. The power fed to each diode is estimated to be 11 dBm. Fig. 6 shows a photograph of the $2 \times 4$ $H$-plane multiplying slot array antenna for which the radiation pattern is already plotted in Fig. 5(g).

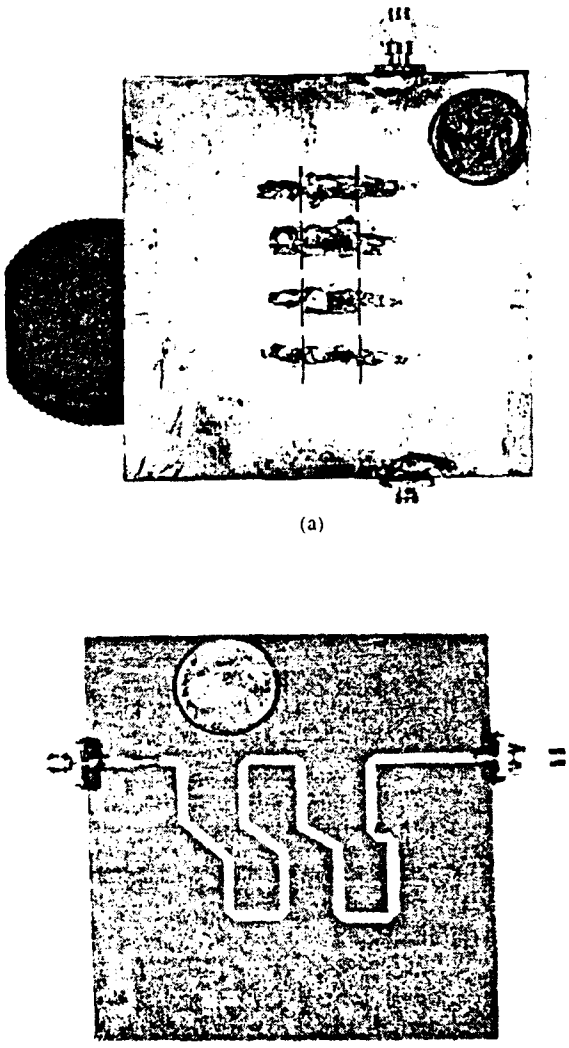


Fig. 6. Pictures of a $2 \times 4$ slot array antenna. (a) Slot array pattern. (b) Microstrip feed pattern.

## IV. Conclusions

By using experimental data which characterize the transition from the microstrip to the slot, we designed a planar multiplier/combiner in the form of a slot array fed by a microstrip on the back side of the substrate. The results show the feasibility of the proposed structure. The new structure has desirable features, such as controllable power coupling and flexibility in array geometry on a planar substrate, as well as the features of a general multiplying slot array [3]. The present structure is suited for microwave and millimeter-wave integrated circuit applications.

## References

[1] K. Chang and C. Sun, "Millimeter-wave power-combining techniques," *IEEE Trans. Microwave Theory Tech.*, vol. MTT-31, pp. 91–107, Feb. 1983.

[2] J. W. Archer and M. T. Faber, "High-output, single- and dual-diode, millimeter-wave frequency doublers," *IEEE Trans. Microwave Theory Tech.*, vol. MTT-33, pp. 533–538, June 1985.

[3] N. Camilleri and T. Itoh, "A quasi-optical multiplying slot array," *IEEE Trans. Microwave Theory Tech.*, vol. MTT-33, pp. 1189–1195, Nov. 1985.

[4] K. C. Gupta, R. Garg, and I. J. Bahl, *Microstrip Lines and Slotlines*. Norwood, MA: Artech House, 1979.
[5] J. B. Knorr, "Slotline transitions," *IEEE Trans. Microwave Theory Tech.*, vol. MTT-22, pp. 548–554, May 1974.
[6] W. L. Stutzman and G. A. Thiele, *Antenna Theory and Design*. New York: Wiley, 1981.

✠

S. Nam was born in Korea on February 2, 1959. He received the B.S. degree in electronic engineering from the Seoul National University in 1981 and the M.S. degree in electrical engineering from the Korea Advanced Institute of Science and Technology in 1983. Since 1986, he has been with the Department of Electrical and Computer Engineering, University of Texas at Austin, where he is working towards the Ph.D. degree in microwave engineering. His research interest is in the area of microwave fields and circuits especially guided-wave structures and their discontinuity effect on microwave circuits.

✠

Tomoki Uwano (M'87) was born in Toyama, Japan, on October 18, 1948. He received the B.S. degree from the Tokyo Institute of Technology in 1971.

Since 1971, he has been employed by the Matsushita Electric Ind. Co., Ltd, Osaka, Japan, where he has been engaged in research and development on microwave and millimeter-wave circuitry and satellite communication. From April 1985 to December 1986, he was a Visiting Scholar in the Department of Electrical and Computer Engineering of the University of Texas at Austin.

Mr. Uwano is a member of the Institute of Electronics, Information and Communication Engineers of Japan.

✠

Tatsuo Itoh (S'69–M'69–SM'74–F'82) received the Ph.D. degree in electrical engineering from the University of Illinois, Urbana, in 1969.

From September 1966 to April 1976, he was with the Electrical Engineering Department, University of Illinois. From April 1976 to August 1977, he was a Senior Research Engineer in the Radio Physics Laboratory, SRI International, Menlo Park, Ca. From August 1977 to June 1978, he was an Associate Professor at the University of Kentucky, Lexington. In July 1978, he joined the faculty at the University of Texas at Austin, where he is now a Professor of Electrical and Computer Engineering and Director of the Electrical Engineering Research Laboratory. During the summer of 1979, he was a guest researcher at AEG-Telefunken, Ulm, West Germany. Since September 1983, he has held the Hayden Head Centennial Professorship of Engineering at the University of Texas. In September 1984, he was appointed Associate Chairman for Research and Planning of the Electrical and Computer Engineering Department.

Dr. Itoh is a member of the Institute of Electronics and Communication Engineers of Japan, Sigma Xi, and Commissions B and D of USNC/URSI. He served as the Editor of the IEEE TRANSACTIONS ON MICROWAVE THEORY AND TECHNIQUES for 1983–1985. He serves on the Administrative Committee of the IEEE Microwave Theory and Techniques Society. Dr. Itoh is a Professional Engineer registered in the state of Texas.

# APPENDIX 4

# CROSSTIE OVERLAY SLOW-WAVE STRUCTURE FOR BROADBAND TRAVELING-WAVE TYPE ELECTRO-OPTICAL MODULATORS*

**H.-Y. Lee, T.H. Wang, T. Itoh**
*Department of Electrical and Computer Engineering*
*The University of Texas at Austin, Austin, TX 78712*

*ABSTRACT*

This paper proposes a new crosstie overlay slow-wave structure for a traveling-wave electro-optical modulator and presents a design method including design considerations for the optimum structure. This structure can be designed to satisfy the phase velocity and impedance matching conditions simultaneously over a broad spectral bandwidth. This idea can be applied to a number of electrode structures for broadband traveling-wave optical modulators.

## INTRODUCTION

Very high-speed optical modulators operating up to millimeter wave frequencies are required for high-bit rate optical communication and high-speed optical signal processing. The direct modulation of semiconductor lasers in that regime is not effective due to the cavity structure and needs a short cavity to maintain the single longitudinal mode.

*This work was supported by the U.S. Army Research Office under contract DAAG-29-84-K-0076.

External laser modulation using optical modulators, however, can be used effectively at such high frequencies while maintaining the cavity mode and high purity spectral characteristics.

In particular, traveling-wave optical modulators are very useful for such external modulation. This is because their modulation depths are linearly proportional to the interaction length of the crystal when there is no phase mismatch between the modulation and light waves along the crystal. In order to maximize their modulation bandwidths, the phase and impedance matching conditions must be kept over a wideband and along the crystal through a proper design of traveling-wave structures[1].

Recently, a two-layer traveling-wave type modulator structure using thin $LiNbO_3$ crystal on a dielectric subtrate was proposed to satisfy the above two matching conditions simultaneously[2]. Since the phase velocity of the modulation wave is much slower than that of the light wave in the case of the $LiNbO_3$ crystal, the velocity of the modulation wave was increased using a substrate layer which has a low dielectric constant and supports the thin $LiNbO_3$ layer. However, such a two-layer structure is intrinsically dispersive because the modulation fields are gradually concentrated into the upper $LiNbO_3$ layer having a high dielectric constant with the increase of frequency.

Although waveguide modulators on semiconductor substrates offer the potential for monolithic integration with sources and electrical driver circuitry, no semiconductor waveguide modulators with traveling-wave electrodes have been reported to date[3]. This is because the electro-optic coefficients of semiconductor materials are relatively small compared to $LiNbO_3$. Their Schottky junction capacitances, depending on the applied voltage, complicate the design of broadband traveling-wave structures. Nevertheless, the low dielectric constants and the small velocity mismatch for both GaAs and InP are very attractive because they allow a narrow electrode spacing for a given charateristic impedance and make the phase velocity matching easy. However, conventional coplanar traveling-wave

electrodes on semiconductor materials cannot be designed to achieve this phase matching because the phase velocity of the modulation wave is in all cases higher than that of the light wave due to the field in the air side.

This paper proposes an almost non-dispersive slow wave structure for a wideband traveling-wave type optical modulator. This structure can be designed to satisfy the phase and the impedance matching conditions simultaneously.

## CROSSTIE OVERLAY SLOW-WAVE STRUCTURE

The proposed slow-wave structure shown in Fig. 1 consists of an infinite array of a more capacitive Section A and a more inductive Section B on the coplanar waveguide[4]. Since the period chosen is much smaller than the propagation wavelength, this structure behaves as a uniform transmission line. In this structure, we can increase the effective capacitance( C ) and inductance( L ) of this transmission line independently

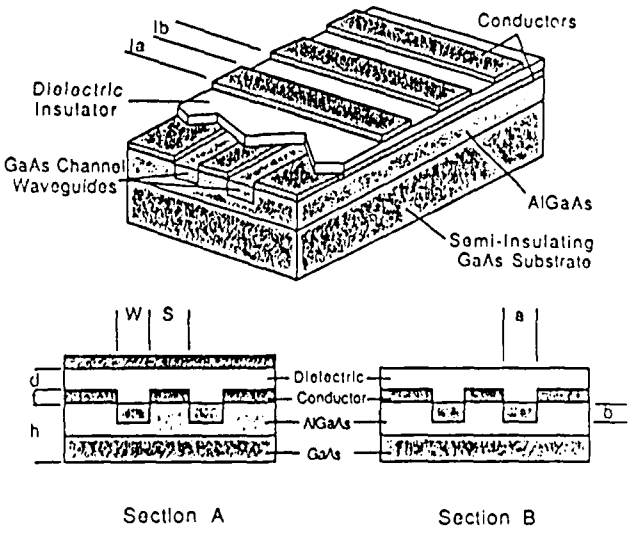


Fig.-1 Proposed Slow-Wave Optical Modulator Structure

by a spatial separation of electric and magnetic energies into two different sections. The shunt capacitance and the series inductance in the equivalent circuit of the transmission line corresponds to the effective capacitance and inductance dorminating in Section A and Section B, respectively. Therefore, the propagation constant( $\beta$ ), which is proportional to $\sqrt{LC}$, can be increased above that of the common coplanar waveguide. The slow-wave factor ( $\beta/\beta_0$,where $\beta_0$ is the free space wavelength ) in the range of from 2.5 to 12 can be obtained with an appropriate design of the structure.

The numerical analysis of this structure has been carried out by a full-wave analysis for each section using the standard spectral domain method[5] and by an application of Floquet's theorem to the periodic array. The dielectric constant is assumed to be uniform in the substrate region at modulating frequencies up to the millimeter wave frequency range, because a small variation of the dielectric constant is enough to form a well guiding optical waveguide. Although the dielectric loss is negligible for the semi-insulating GaAs substrate, the conductor loss cannot be neglected in this small device structure. The real and imaginary parts of the complex propagation constants corresponding to the phase and the attenuation constants can be calculated using the spectral domain analysis and the incremental inductance formula[6], respectively.

While the calculated complex propagation constants( $\beta_A$,$\beta_B$ ) of Section A and Section B are close to each other and below that of the light wave in the channel waveguide, the overall propagation constant( $\beta$ ) of the periodic array that was calculated using the Floquet's theorem can be increased by the different characteristic impedances of the two sections. The following dispersion and impedance equations are derived by applying the Floquet's theorem and continuity conditions of voltage and current at each period junction. The discontinuity effects at the junction are assumed to be small for the simplification.

$$\cos(\gamma l) = \cos(\gamma_A l_A)\cos(\gamma_B l_B) - (1/2)(Z_A/Z_B + Z_B/Z_A)\sin(\gamma_A l_A)\sin(\gamma_B l_B)$$

$$Z = \left[ \frac{Z_A \sin(\gamma_A l_A)\cos(\gamma_B l_B) + Z_B \cos(\gamma_A l_A)\sin(\gamma_B l_B)}{(1/Z_A)\sin(\gamma_A l_A)\cos(\gamma_B l_B) + (1/Z_B)\cos(\gamma_A l_A)\sin(\gamma_B l_B)} \right]^{1/2}$$

where $\gamma$, $Z$ = overall complex propagation constant and characteristic impedance

$\gamma_A$, $\gamma_B$ = complex propagation constant of Sections A and B, respectively

$Z_A$, $Z_B$ = characteristic impedances of Sections A and B, respectively

$l = l_A + l_B$, with $l_A$ and $l_B$ being the lengths of Sections A and B, respectively

Assuming for simplicity that $\gamma_A l_A$, $\gamma_B l_B \ll 1$, $\gamma_A \approx \gamma_B$ and $Z_A \ll Z_B$ the above equations can be reduced to the following simple expressions

$$(1+T)\beta \approx \beta_A (1 + TK + T^2)^{1/2}$$

$$(1+T)^2 \alpha \approx (\beta_A/\beta)[\alpha_A + T^2 \alpha_B + KT(\alpha_A + \alpha_B)/2]$$

$$Z \approx [Z_A Z_B T K/(K+T)]^{1/2}$$

Since $\beta$ and $Z$ are approximately proportional to $\sqrt{Z_B/Z_A}$ and $\sqrt{Z_A Z_B}$ respectively, in the event of $1 \ll Z_B/Z_A$ and $l_A \approx l_B$, we can easily increase the propagation constant while maintaining a given characteristic impedance. Therefore, this property can be applied very effectively in order to achieve the simultaneous matching of the phase and the impedance, that is required in the optimum electrode design of traveling-wave optical modulators. Furthermore, since this slow-wave structure is almost dispersionless due to the uniform transmission line behavior, the structure is very useful for the design of wideband traveling-wave optical modulators. This slow-wave phenomenon can also

be applied to a number of traveling-wave electrode structures for the optimum design of a wideband optical modulator.

## PHASE MATCHED OPTICAL MODULATOR

The proposed slow-wave optical modulator can be fabricated as follows as shown in Fig.1. An AlGaAs layer is grown on a semi-insulating GaAs substrate. GaAs optical channel waveguides are formed on the AlGaAs layer by a buried structure technique[7]. Coplanar waveguide electrodes are fabricated on the top surface of the AlGaAs layer. Next, an insulating dielectric layer is deposited. Finally, periodic metal crosstie overlays are fabricated on the dielectric layer. Therefore, the dielectric loss of the modulation wave and the optical loss due to free carrier absorption can be avoided in this structure. The localized effective index change( $\delta n \sim n^3 r E/2$ ), which is formed by the electro-optic effect for the traveling electric field( E ) of the modulation wave, generates the local phase shift of the optical wave over the interaction length( L )[1]. In order to accumulate the local phase shift along the waveguide, the phase matching between the optical and modulation waves can be accomplished by our proposed slow-wave structure.

### Design of Slow-Wave Coplanar Electrode

This slow-wave structure has many design parameters including a coplanar waveguide, overlay crossties and a dielectric layer. This allowes a wide design flexibility for the simultaneous matching of the phase velocity and the impedance.

The two design requirements for the simultaneous matching of the phase velocity and the impedance are given by

$$Z = 50\ (\Omega)$$

$$n^m_e = n^l_c$$

where $n^m_e$ and $n^l_e$ are the effective index of the modulation and light waves, respectively.

Additional design considerations[3] should be included for high modulation efficiency, low conductor loss and realizable dimensions. High field intensity can be achieved by the minimum realizable electrode gap while low current density requires thick and wide electrodes. Since the applied electric fields in sections A and B are mostly concentrated in dielectric and substrate layers, respectively, it is necessary to increase the length ratio between the two sections( $l_B/l_A$ ) in order to achieve the high effective overlap between the applied field and the optical mode. The one period length( $l_A+l_B$ ) for a fixed ratio( $l_B/l_A$ ) affects only the bandwidth and is limited by the minimum achievable feature size of electrodes. Silicon Nitride is chosen for a dielectric material because of its high dielectric constant and high field strength which allow high slow-wave effect and high field operation, respectively.

## Design of Optical Channel Waveguide

The optical waveguide must be designed interactively with the electrode design to enhance the field efficiency of the modulation wave. The main factors for the optimum design are the effective index, the mode size and the relatve alignment to the electrodes.

Since the composition ratio( x ) of the $Al_xGa_{1-x}As$ layer can be accurately controlled over a wide range using epitaxial growing techniques, the refractive index difference( $\Delta n \approx 0.62\ \Delta x$, where $\Delta x$ is the composition ratio difference ) between GaAs channel and AlGaAs clad of the waveguide can be made large enough for the high field confinement of the optical mode[8]. The mode penetration into the dielectric layer is also quite small due to the high refractive index difference between the dielectric and the GaAs layers. Therefore, the effective index( $n^l_e$ ) and the horizontal and the vertical mode sizes( $w_h, w_v$ ) can be simply expressed as shown

below for the well guided fundamental mode in rectangular waveguides[9].

$$n^{l}_{c} = [\, n_1^2 - (\lambda / 2a)^2 - (\lambda / 2b)^2 \,]^{1/2}$$

$$w_h = a + 0.23\,\lambda / (\Delta n \cdot n_2)^{1/2}$$

$$w_v = b + 0.12\,\lambda / (\Delta n \cdot n_2)^{1/2}$$

where $n_1$, $n_2$ = refractive index of GaAs channel and AlGaAs clad ,respectively

a, b = horizontal and vertical length of the rectangular waveguide ,respectively

$\lambda$ = free space wavelength of the optical wave

Although small mode size and low effective index are advantageous for high field overlap and easy phase matching, the minimum mode size should be comparable with those of typical single mode fibers ($\approx 7\,\mu m$) for low fiber coupling loss. Therefore, in the optimum design there is a tradeoff between the high field overlap and the low coupling loss. Since the minimum electrode gap in this structure is limited by the impedance matching to 10 μm, the practical ratio between the mode size and the electrode gap lies around 0.7. Therefore, the waveguide placed between the electrodes, which uses the horizontal component of the modulation field, is effective for high field overlap( $\Gamma \approx 0.6$ ) and has low optical loss[10].

## NUMERICAL RESULTS AND DISCUSSION

There are many possible combinations of multiple design parameters for the simultaneous matching of the phase velocity and impedance. One combination listed in Table-1 is obtained through the above mentioned design considerations and the numerical calculations.

Table-1 Design Parameters for the Slow-Wave Modulator

| | MATERIAL | DIMENSION ($\mu$m) | PROPERTY |
|---|---|---|---|
| SUBSTRATE | SEMI-INSULATING GaAs | h = 100 | $\varepsilon_r$ = 12.9 |
| DIELECTRIC | $Si_3N_4$ | d = 0.8 | $\varepsilon_r$ = 6.8 |
| OPTICAL WAVEGUIDE | GaAs CHANNEL | a = 6.5 ,b = 3.0 | $n_1$ = 3.43 |
| | AlGaAs CLAD | | $n_2$ = 3.33 |
| ELECTRODE | Au | W = 11<br>S = 6<br>$l_A$ = 2<br>$l_B$ = 17<br>t = 3 | $R_S = 3\times 10^{-7}\sqrt{f}$ ($\Omega$/sq) |

Table-2 Numerical Results for the Design of Table-1
(at 1 GHz modulation frequency and 1.15 $\mu$m light wavelength)

| | SECTION A | SECTION B | OVERALL |
|---|---|---|---|
| $n_e^m$ | 2.74 | 2.72 | 3.42 |
| $\alpha_v$ (cm$^{-1}$) | 0.40 | 0.16 | 0.28 |
| Z ($\Omega$) | 8.1 | 66 | 50 |
| $n_e^l$ | 3.42 | | |
| $w_h$ | 7.0 ($\mu$m) | | |
| $w_v$ | 3.2 ($\mu$m) | | |
| $V_{min}^{\pi}$ | 10 (V) | | |
| 3 dB f·L | 320 (GHz · cm) | | |

## Bandwidth

The effective index dispersion and the characteristic impedance change for the design in Table-1 are shown in Fig-2. From this figure it can be seen that this slow-wave optical modulator has a very wide bandwidth for the simultaneous phase and impedance matching. In order to see the frequency characteristics more clearly, we refer to the phase-modulation reduction factor[11] given by

$$\eta = \sin(u)/u$$

$$u = \pi f L (n^{m}_{e}(f) - n^{l}_{e})/c$$

where f, L and c are the modulation frequency, the modulator length and the free space velocity, respectively. In Fig-3 the phase-modulation reduction factor ($\eta$) is plotted against the frequency-length product f(GHz)·L(cm). The frequency-length product at the 3 dB phase-modulation factor is about 320 (GHz·cm), which is about 50 times larger than those of normal $LiNbO_3$ modulators and 7 times larger than that of a phase matched $LiNbO_3$ modulator[2]. Therefore, this modulator can be operated up to the bandwidth of 320 GHz for the modulator length of 1 cm.

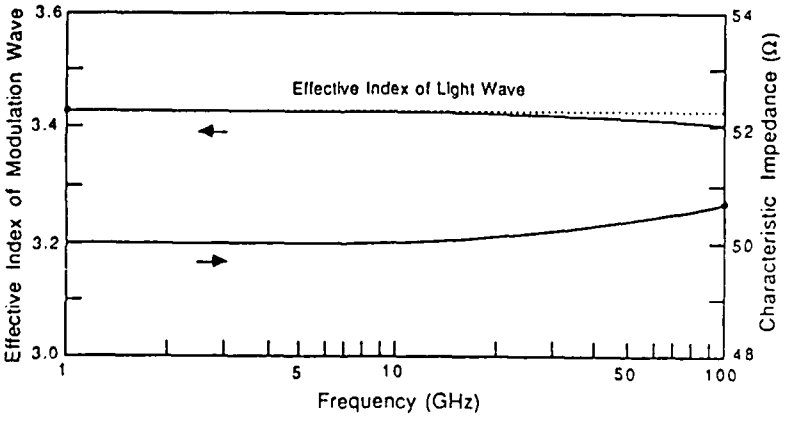


Fig.- 2 Dispersion and Impedance Characteristics

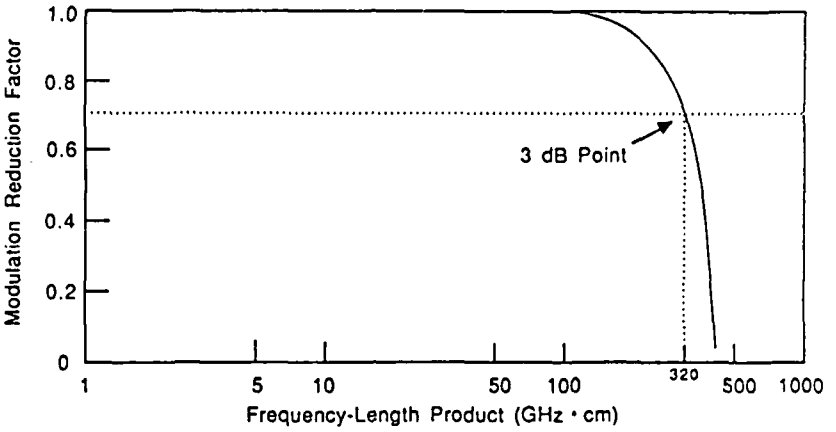


Fig-3 Phase-Modulation Reduction Factor

## Conductor Loss and Modulation Voltage

The overall conductor loss per unit length of this structure is about two times larger than that of the common CPW due to the slow-wave factor and the high conductor loss in cross-tie section. Therefore, the effective interaction length ( $L_{eff}$ ) is reduced from the actual length( L ) as below in the phase matched case.

$$L_{eff} = ( 1 - e^{-\alpha_v L} ) / \alpha_v$$

where $\alpha_v$ is the voltage attenuation constant.

The maximum effective length for the infinitely long modulator( $L = \infty$ ) is the inverse of the attenuation constant. Therefore, the minimum voltage required for the half-wave modulation( $\Delta\beta = \pi$ ) of this modulator can be given by the following equation in the case of perfect phase matching.

$$V\pi_{min} = \lambda G \alpha_v / n^3 r \Gamma$$

Although the theoretical $V\pi_{min}$( $\approx$ 10 V at 1GHz ) is a litttle larger than those of the $LiNbO_3$ modulators having assymmetric coplanar electrodes[12], it can be reduced by using the assymmetric coplanar

slow-wave structure. That allows a smaller electrode gap for a given characteristic impedance.

## CONCLUSIONS

In this paper, a new crosstie overlay slow-wave structure is proposed for wideband traveling-wave type optical modulators. The simultaneous matching of phase veloity and impedance has been successfully achieved through the numerical analysis of the slow-wave electrode structure and the design of the optical modulator. This simultaneous matching can be accomplished over a wide bandwidth due to the uniform transmission line behavior of the proposed electrode structure.

## REFERENCES


[1] R. C. Chen, *Proceedings of the IEEE*, Vol. 58, pp. 1440-1457, October 1970.

[2] K. Atsuki and E. Yamashita, *J. of Lightwave Tech.*, Vol. LT-5, pp. 316-319, March 1987.

[3] R. Alferness, *IEEE Trans. Microwave Theory Tech.*, Vol. MTT-30, pp. 1121-1137, August 1982.

[4] T. H. Wang and T. Itoh, *1987 IEEE International Microwave Symposium Digest*, Vol. 1, pp. 315-318, June 1987.

[5] T. Itoh, *IEEE Trans. Microwave Theory Tech.*, Vol. MTT-28, pp. 733-736, July 1980.

[6] R. A. Pucel *et al.*, *IEEE Trans. Microwave Theory Tech.*, Vol. MTT-16, pp. 342-350, 1968.

[7] K. Saito and R. Ito, *IEEE J. of Quantum Electr.*, QE-16, pp. 205-215, February 1980.

[8] S. Adachi, *J. Appl. Phys.*, Vol.58(3), pp. R1-R29, 1 August 1985.

[9] E. A. J. Marcatili, *Bell Sys. Tech. J.*, pp. 2071-2103, September 1969.

[10] D. Marcuse, *IEEE J. of Quantum Electr.*, QE-18, pp. 393-398, March 1982.

[11] L. P. Kaminow and J. Liu, *Proceedings of the IEEE*, Vol. 51, pp. 132-136, January 1963.

[12] R. C. Alferness *et al., Electron. Lett.*, Vol. 13, pp. 309-310, March 1986.

END

DATE

FILMED

DTIC

JULY 88